New Phytologist

Research

m^{6}A demethylase OsALKBH5 is required for double-strand break formation and repair by affecting mRNA stability in rice meiosis

Feiyang Xue[1]*, Jie Zhang[1]*, Di Wu[2]*, Shiyu Sun[1], Ming Fu[1], Jie Wang[1], Iain Searle[3], Hongbo Gao[2] and Wanqi Liang[1,4]

[1]Joint International Research Laboratory of Metabolic & Developmental Sciences, State Key Laboratory of Hybrid Rice, School of Life Sciences and Biotechnology, Shanghai Jiao Tong University, Shanghai, 200240, China; [2]Joint Center for Single Cell Biology, School of Agriculture and Biology, Shanghai Jiao Tong University, Shanghai, 200240, China; [3]Department of Molecular and Biomedical Sciences, School of Biological Sciences, The University of Adelaide, Adelaide, SA, 5005, Australia; [4]Yazhou Bay Institute of Deepsea Sci-Tech, Shanghai Jiao Tong University, Sanya, 572024, China

Authors for correspondence:
Wanqi Liang
Email: wqliang@sjtu.edu.cn

Hongbo Gao
Email: hongbo.gao@sjtu.edu.cn

Received: *1 January 2024*
Accepted: *13 June 2024*

New Phytologist (2024)
doi: 10.1111/nph.19976

Key words: DSB, m^{6}A, meiosis, OsALKBH5, rice.

Summary

- N^6-methyladenosine (m^{6}A) RNA modification is the most prevalent messenger RNA (mRNA) modification in eukaryotes and plays critical roles in the regulation of gene expression. m^{6}A is a reversible RNA modification that is deposited by methyltransferases (writers) and removed by demethylases (erasers). The function of m^{6}A erasers in plants is highly diversified and their roles in cereal crops, especially in reproductive development essential for crop yield, are largely unknown.
- Here, we demonstrate that rice OsALKBH5 acts as an m^{6}A demethylase required for the normal progression of male meiosis.
- OsALKBH5 is a nucleo-cytoplasmic protein, highly enriched in rice anthers during meiosis, that associates with P-bodies and exon junction complexes, suggesting that it is involved in regulating mRNA processing and abundance. Mutations of *OsALKBH5* cause reduced double-strand break (DSB) formation, severe defects in DSB repair, and delayed meiotic progression, leading to complete male sterility. Transcriptome analysis and m^{6}A profiling indicate that OsALKBH5-mediated m^{6}A demethylation stabilizes the mRNA level of multiple meiotic genes directly or indirectly, including several genes that regulate DSB formation and repair.
- Our study reveals the indispensable role of m^{6}A metabolism in post-transcriptional regulation of meiotic progression in rice.

Introduction

N^6-methyladenosine (m^{6}A) is an important covalent base modification in DNA and RNA of many organisms, and plays important roles in cell specification and cell fate determination (Zheng *et al.*, 2013; Li *et al.*, 2014; Wang *et al.*, 2014; Fu *et al.*, 2015; Greer *et al.*, 2015; Zhang *et al.*, 2015; C. Zhang *et al.*, 2017; S. Zhang *et al.*, 2017; Xiao *et al.*, 2018; Zhou *et al.*, 2018). m^{6}A is the most abundant internal post-transcriptional modification in messenger RNA (mRNA) and displays broad functions in the regulation of mRNA metabolism and processing such as splicing (Zhao *et al.*, 2014; Tang *et al.*, 2018), nuclear export (Zheng *et al.*, 2013), stability (Wang *et al.*, 2014; Liu *et al.*, 2018; Tang *et al.*, 2018; Wei *et al.*, 2018), translation (Meyer *et al.*, 2015; Wang *et al.*, 2015), and protein–RNA interactions (Liu *et al.*, 2015).

The m^{6}A modification is reversible and dynamically written, read, and erased by a series of proteins. In mammals, m^{6}A deposition is carried out by a methyltransferase complex (MTC), a multiprotein complex with a core catalytic part comprising METTL3 (methyltransferase-like 3)–METTL14 (methyltransferase-like 14)–WTAP (Wilms' tumor 1-associating protein) (Liu *et al.*, 2014; Ping *et al.*, 2014). 'Reader' proteins with YT521-B homology (YTH) domains recognize and bind to m^{6}A sites, thereby controlling the stability and translation of mRNA (Wang *et al.*, 2015; Du *et al.*, 2016; Xiao *et al.*, 2016; Hsu *et al.*, 2017; Shi *et al.*, 2017). A group of proteins belonging to the 2-oxoglutarate and Fe^{2+} (2OG–Fe (II))-dependent oxygenase superfamily have been identified as m^{6}A demethylases. Two well-known examples are ALKBH5 (α-ketoglutarate-dependent dioxygenase alkB homolog 5) and FTO (fat mass and obesity-associated protein; Jia *et al.*, 2011; Zheng *et al.*, 2013). Investigations of these writers, readers, and erasers in various animal species indicate broad, divergent, and crucial functions of m^{6}A in oocyte maternal-to-zygotic transition, spermatogenesis, tumorigenicity, and other developmental processes (Zheng *et al.*, 2013; S. Zhang *et al.*, 2017; Zhao *et al.*, 2017; Chang *et al.*, 2020; C. Zhang *et al.*, 2017; Z. Zhang *et al.*, 2020; Wu *et al.*, 2022). In mice, m^{6}A deposition and removal machineries

*These authors contributed equally to this work.

regulate meiosis initiation, meiotic progression, and spermatogenesis, respectively (Zheng *et al.*, 2013; Xu *et al.*, 2017).

As in animals, the m^6A modification in plants is also reversible and can be written, read, and removed. *Arabidopsis* MTA (the homolog of human METTL3) was the first characterized m^6A mRNA methyltransferase in plants, inactivation of which led to failure of embryo development at the globular stage (Zhong *et al.*, 2008). Other m^6A methyltransferase subunits, including MTB, FIP37, VIRILIZER, HAKAI, and the newly discovered FIONA1, which are homologs of human METTL14, WTAP, KIAA1429, HAKAI, and METTL16, respectively, have also been identified and shown to play critical roles in plant morphogenesis (Zhong *et al.*, 2008; Shen *et al.*, 2016; Růžička *et al.*, 2017; Xu *et al.*, 2022). In rice, OsFIP37 (also named OsFIP) is a component of the MTC, essential for microspore generation and development (F. Zhang *et al.*, 2019; Cheng *et al.*, 2022). Two YTH-domain reader proteins, ECT2 and ECT3, have been demonstrated to bind m^6A sites and control trichome branching, leaf emergence time, and morphology in *Arabidopsis* (Arribas-Hernández *et al.*, 2018; Scutenaire *et al.*, 2018; Wei *et al.*, 2018). ALKBH9B and ALKBH10B are m^6A demethylases in *Arabidopsis*, and their mutants affect plant defense against viral infection, floral transition, and vegetative growth (Duan *et al.*, 2017; Martínez-Pérez *et al.*, 2017). Another demethylase, SIALKBH2 (also named SIALKBH9A), modulates the stability of targeted m^6A transcripts during tomato fruit ripening (Zhou *et al.*, 2019; Shen *et al.*, 2022). These results demonstrate critical and diverse functions of m^6A methylation during plant development, although a role for OsFIP37 in the early generation of microspores was recently shown (F. Zhang *et al.*, 2019; Cheng *et al.*, 2022), there is little information about the role of m^6A modification in plant reproductive development.

Meiosis is a specialized form of cell division for haploid gametophyte generation, consisting of one round of DNA replication and two rounds of cell division. Homologous pairing, synapsis, recombination, and crossover (COs) formation occur in Prophase I, and are particularly important to ensure accurate separation of homologous chromosomes. Meiotic recombination is initiated by programmed double-stranded break (DSB) formation, catalyzed by the evolutionarily conserved type-II DNA topoisomerase SPO11-1/TOP6A1 (topoisomerase VIA) and MTOPVIB (topoisomerase VIB) complex (Bergerat *et al.*, 1997; Vrielynck *et al.*, 2016). The DSB ends are resected by the Mre11-Rad50-Xrs2 (MRX) (meiotic recombination 11 (Mre11)-radiation sensitive 50 (RAD50)-X-ray-sensitive 2 (Xrs2)) and SAE2 (SUMO-activating-enzyme 2) ensemble to yield 3′ single-stranded DNA overhangs (Cannavo *et al.*, 2019), which are bound by RPA (replication protein A), RAD51, and DMC1 to promote homology search, resulting in strand exchange and formation of a stable single-end invasion (SEI) intermediates (Hinch *et al.*, 2020). The SEI intermediates can be stabilized by ZMM proteins and their interactors that are eventually resolved as CO or non-crossovers (NCO) (Bishop & Zickler, 2004; Chelysheva *et al.*, 2012; Shen *et al.*, 2012; Li *et al.*, 2018; J. Zhang *et al.*, 2019).

To date, numerous proteins have been identified as regulators of meiotic Prophase I. In rice, reproductive phasiRNAs are essential for the elimination of specific RNAs during Prophase I (Jiang *et al.*, 2020; Y. C. Zhang *et al.*, 2020); while RNA-dependent RNA polymerase 6 (RDR6) is a core factor in small RNA biogenesis and vital for rice meiotic DSB formation (Liu *et al.*, 2020). Recently, it has been reported that OsFIP37 deposits m^6A on mRNAs to regulate meiotic progression in rice (F. Zhang *et al.*, 2019; Cheng *et al.*, 2022), but whether m^6A demethylation is also involved in controlling the dynamics of meiocyte transcripts is yet unknown.

In this study, we have identified the 2OG-Fe (II) domain protein OsALKBH5 as an m^6A-mRNA demethylase essential for male fertility. Its protein levels and localization in the anther are consistent with a role in male meiocyte development. Mutation of *OsALKBH5* resulted in altered m^6A levels and decreased stability of transcripts required for early meiotic events of the microsporocyte, leading to defective chromosome behaviors and sterility. Our findings demonstrate that mRNA methylation and OsALKBH5 play critical roles in proper DSB formation and repair during rice meiosis.

Materials and Methods

Plant materials

All rice plants (*Oryza sativa* L.) were grown in the paddy field of Shanghai Jiao Tong University, located in Shanghai (31.03°N, 121.45°E), China. The *Osalkbh5* mutants were isolated from an existing rice mutant library in *O. sativa* L. ssp. *japonica* cv 9522 created by ^{60}Co γ-rays (Chen *et al.*, 2006). The F_2 mapping populations were generated from a cross between *Osalkbh5* and cv Guang Lu Ai 4 (ssp. *indica*). Tobacco (*Nicotiana benthamiana* L.) plants were grown in the glasshouse under 16 h : 8 h, light : dark conditions.

Characterization of mutant phenotypes

Photographs of plants, flowers, anthers, and pollen, as well as semi-thin cross-section were performed according to the previous studies (Li *et al.*, 2006, 2020). Anthers of different developmental stages were collected based on spikelet and anther length according to the described cytological changes by Zhang *et al.* (2011).

For analysis of chromosome behavior, fresh rice panicles containing meiotic spikelets were fixed with Carnoy's solution (3 : 1 (v/v) ethanol : glacial acetic acid) for 4′,6-diamidino-2-phenylindole (DAPI) staining and fluorescent *in situ* hybridization (FISH) assays, or 4% (w/v) paraformaldehyde for immunolocalization, and prepared as described previously (He *et al.*, 2016; Wang *et al.*, 2017). FISH probes to rice 5s rDNA and centromere were generated and assayed as described previously (J. Zhang *et al.*, 2019). For immunolocalization, antibodies against rice meiotic protein (γH2AX, OsREC8, OsCOM1, PAIR2, PAIR3, OsZEP1, OsZIP4, and OsHEI10) were generated and assayed as described previously (Fu *et al.*, 2016, 2020; He *et al.*, 2016; Wang *et al.*, 2017; J. Zhang *et al.*, 2019). After counterstaining with DAPI, meiotic chromosomes were photographed using the Eclipse Ni-E microscope

(Nikon Precision, Tokyo, Japan), and analysis performed using NIS-ELEMENTS Advanced Research software. Image deconvolution was carried out using the function 'Mexican Hat' before counting the number of dot-like immunofluorescence signals.

Cloning of *OsALKBH5* and complementation

Bulked segregant analysis was used using InDel (insertion–deletion) markers developed by our laboratory. Two *Osalkbh5* mutants were first mapped between two InDel markers LY603 (located on AP001129) and LY604 (located on AP007226). A further 4 InDel markers WJ603-2, WJ603-3, FY-1, and WJ603-5 (located on AP003456, AP002542, AP003487, and AP002536, respectively) were designed and used to further narrow the mapping region. *Osalkbh5* mutants were finally mapped to between WJ603-3 and FY-1.

High-throughput sequencing of *Osalkbh5* leaves from the F_2 population was used to verify mutations. A 1-bp insertion in Exon 1 (*Osalkbh5-1*) and 2-bp deletion in Exon 5 (*Osalkbh5-2*) of *Os06g0138200* were found to cause premature translation termination.

To verify whether *Os06g0138200* was responsible for the *Osalkbh5* phenotype, a 7266-bp genomic fragment containing a 2868-bp upstream promoter region, 3902-bp *OsALKBH5* genomic sequence, and 496-bp downstream region was amplified from cv 9522 genomic DNA. The genomic fragment was inserted into the binary vector pCAMBIA1301. Meanwhile, *OsALKBH5-eGFP* was constructed by fusing an in-frame enhanced green fluorescent protein (GFP) to the C-terminus. Calli induced from young panicles of homozygous *Osalkbh5* plants were used for transformation with *Agrobacterium tumefaciens* EHA105, and polymerase chain reaction was used to identify positive transgenic lines. We obtained 45 and 37 transgenic lines respectively. Among them, 44/45 and 31/37 transgenic plants could produce seeds normally. Primers used for map-based cloning and vector construction are listed in Supporting Information Table S1.

Phylogenetic analysis

The full-length protein sequence of OsALKBH5 (616 aa) was used for a BLASTP search for plants homologs in PHYTOZOME (https://phytozome-next.jgi.doe.gov). Homologous sequences were screened from monocots rice (*O. sativa* L.), *Brachypodium distachyon* L., maize (*Zea mays* L.), and dicots *Arabidopsis* (*Arabidopsis thaliana* L.), soybean (*Glycine max* L.), and tomato (*Solanum lycopersicum* L.). Protein sequences from human (*Homo sapiens*) ALKBH1–8 and FTO and *Escherichia coli* EsALKB were also retrieved from NCBI (https://www.ncbi.nlm.nih.gov/). Sequences alignments were conducted by CLUSTALW and generated by ESPRIPT v.3.0 (https://espript.ibcp.fr/ESPript/ESPript/index.php). The phylogenetic trees were generated using the neighbor-joining method via the MEGA5 software.

RT-qPCR

Total RNA was isolated from rice tissues (seedling root, seedling leaf, palea/lemma, and anthers at different stages) using TRNzol Universal RNA Reagent (Tiangen Biotech, Beijing, China) according to the manufacturer's instructions. Two micrograms of total RNA was used to synthesize first-strand cDNA with the Tiangen FastKing RT Kit (with gDNase). Reverse transcription quantitative polymerase chain reaction (RT-qPCR) analysis was performed using a CFX96™ Real-Time System (Bio-Rad) or LightCycler® 96 (Roche Biotech, Basel, Switzerland) with 2 × SuperReal PreMix Plus (with SYBR Green I) (Tiangen Biotech) or 2 × SYBR Green *Pro Taq* HS Premix (Accurate Biology, Hunan, China). Expression levels were calculated relative to *OsActin* (Os03g0718100). All reactions were performed with three biological replicates, and data plotted as mean ± SD.

OsALKBH5 antibody preparation and Western blot

The OsALKBH5 polyclonal antibody was prepared by Abclonal (Wuhan, China). A 633-bp DNA fragment encoding a 211 aa peptide of OsALKBH5 (residues 406–616) was amplified from rice cDNA and cloned into the protein expression vector pGEX-4T-1. The recombinant protein was expressed in *E. coli* Rosetta (DE3), purified, and used to produce rabbit polyclonal antibodies. Protein of rice tissues was isolated from the remaining components after RNA extraction according to the manufacturer's instructions and diluted to equal concentration. Then, Western blot with anti-OsALKBH5 antibody (1 : 1500 dilution) was performed, and anti-tubulin antibody (Beyotime Biotech, Shanghai, China; 1 : 2000 dilution) was used as the control.

Subcellular localization and colocalization of OsALKBH5

The coding sequence of *OsALKBH5* was cloned from cDNA of cv 9522 and cloned into pA7-eGFP and PHB-YFP vectors, while *OsMago1* and *OsDCP1-1* were cloned into PHB-mCherry vectors. Rice protoplasts were isolated from etiolated hypocotyls of 12 d old rice plants, and transformation performed using the polyethylene glycol-mediated transient method as described (Bart *et al.*, 2006; Yoo *et al.*, 2007). For transient transformation in tobacco leaves, *A. tumefaciens* strain GV3101 was used and transformed as described (Liu *et al.*, 2010). Fluorescence signals were observed using confocal laser-scanning microscopy (Leica TCS SP5; Leica Microsystems, Wetzlar, Germany) at wavelengths: for eGFP, excitation 488 nm and emission 500–550 nm; for YFP, excitation 514 nm and emission 530–580 nm and for mCherry, excitation 594 nm and emission 600–640 nm.

Protein expression and purification

The *OsALKBH5* coding sequence was amplified and inserted into pET-28a (+), which adds a 6 × His tag to the protein N-terminus. Human *ALKBH5* (missing the first 198 bp) was ligated into pET-28a (+) as a positive control. Vectors were transformed into *E. coli* Rosetta (DE3), cultured in Luria-Bertani (LB) medium with 50 mg l^{-1} kanamycin at 37°C until OD_{600} 0.6–0.8. Protein expression was induced with 0.4 mM isopropyl-β-D-thiogalactoside (IPTG) at 16°C overnight. Tagged proteins were purified on a Ni^{2+}-chelating sepharose column

(Thermo Fisher Scientific, Waltham, MA, USA) following the manufacturer's instructions.

In vitro ALKBH5 activity assay

The biochemical activity assay was performed as reported (Jia *et al.*, 2011) with minor modifications. Briefly, the reaction mixture, containing 5 μg RNA with m^6A, 0.3 nmol ALKBH5, 100 mM KCl, 2 mM $MgCl_2$, 0.2 U μl^{-1} RNasin, 2 mM L-ascorbic acid, 300 μM α-ketoglutarate, 150 μM $(NH_4)_2Fe(SO_4)_2{\cdot}6H_2O$, and 50 mM HEPES buffer (pH 7.0), was incubated at room temperature for 2.5 h and then quenched by adding 5 mM EDTA followed by heating at 95°C for 10 min. RNA was digested with 2 U nuclease P1 and 2 U alkaline phosphatase at 37°C for 2 h. After extraction with chloroform, 10 μl supernatant was analyzed on a UPLC system (Agilent Tech, Santa Clara, CA, USA) equipped with an ACQUITY UPLC BEH C18 1.7 μm analytical column (2.1 × 100 mm; Waters, Milford, MA, USA), eluted with buffer A (5 mM ammonia acetate) and buffer B (60% acetonitrile, 5 mM ammonia acetate) with a flow rate of 0.3 ml min^{-1} at room temperature. The detection wavelength was set at 260 nm.

Quantitative analysis of m^6A levels

Total RNA was isolated from meiotic wild-type (WT) and *Osalkbh5* anthers using TRNzol Universal RNA Reagent, and mRNA extracted using the Dynabeads™ mRNA DIRECT™ Kit (Invitrogen). One hundred nanogram mRNA was digested as described (Jia *et al.*, 2011) and analyzed on a UPLC system as described above.

Dot-blot analysis of the total m^6A levels

mRNAs extracted from WT and mutant anthers were serially diluted to 500, 100, and 20 ng μl^{-1}. After denatured at 95°C for 3 min and chilled on ice, 2 μl mRNA of each dilution was used for dot-blot assay following the protocol as described by Shen *et al.* (2017).

MeRIP-seq analysis

MeRIP-Seq was performed by Cloudseq Biotech Inc. (Shanghai, China) as described (Meyer *et al.*, 2012) with slight modifications. Briefly, fragmented RNA isolated from meiotic anthers was incubated with anti-m^6A polyclonal antibody (202003; Synaptic Systems, Goettingen, Germany) in IPP buffer for 2 h at 4°C. The mixture was then immunoprecipitated by incubation with protein-A beads (Thermo Fisher Scientific) at 4°C for 2 h. Bound RNA was eluted from the beads with m^6A (PR3732; Berry & Associates, Dexter, MI, USA) in IPP buffer and extracted with TRIzol reagent (Thermo Fisher Scientific) according to the manufacturer's instruction. Purified RNA was used for RNA-seq library generation with NEB Next® Ultra™ II Directional RNA Library Prep Kit (New England Biolabs, Ipswich, MA, USA). Both the input sample without immunoprecipitation and the m^6A IP samples were subjected to 150-bp paired-end sequencing on an Illumina HiSeq sequencer (Illumina, San Diego, CA, USA).

HiSeq reads were quality controlled (threshold Q30) using the CUTADAPT software (v.1.9.3) to remove 3′ adaptors and low-quality reads. Trimmed reads were aligned to the reference genome (UCSC HG19) with the HISAT2 software (v.2.0.4), the MACS software (v.1.4.2) was used for m^6A peak calling, and the DIFFREPS software was used to identify differentially enriched m^6A peaks. Peaks were annotated with home-made scripts. Gene Ontology (GO) analysis was performed for differentially expressed genes (DEGs) and differentially methylated genes (DMEs). Read alignments were visualized by using INTEGRATIVE GENOMICS VIEWER.

RNA-Seq and analysis

Three biological replicates were taken for each single cell type. RNA library was directly constructed from meiocytes collected in a 1.5-ml tube, using the TruePrep Index Kit v.2 for Illumina (Vazyme, Nanjing, China). Sequencing data were processed by use of the following software: BOWTIE, TRIMGALORE, SAMTOOLS, HISAT2, MARKDUPLICATES, and DESEQ2. The whole-genome sequence and annotation were downloaded from The Rice Annotation Project Database (RAP-DB, http://rapdb.dna.affrc.go.jp).

RIP-qPCR analyses

RIP-qPCR was performed as described (Xing *et al.*, 2015) using GFP beads and florets at meiosis stage from complemented plants.

Results

Osalkbh5 mutants are completely male sterile

Two allelic male-sterile mutants, *Osalkbh5-1 and Osalkbh5-2*, were identified from an existing gamma-irradiated mutant M_2 library in rice cultivar 9522 (*O. sativa* L. ssp. *japonica*). Both mutant plants were indistinguishable from WT plants during vegetative growth (Fig. 1a), but, at the reproductive stage, showed thin, pale-yellow anthers (Fig. 1b,c) containing no viable pollen (Fig. 1d). When mutant flowers were pollinated with WT pollen, they produced a similar number of seeds to WT, indicating that female fertility was not affected. Segregation analysis of self-fertilized heterozygous plants showed a 3 : 1 ratio (fertile : sterile, *Osalkbh5-1* (51 : 18), $\chi^2 = 0.04$, $P > 0.05$; *Osalkbh5-2* (63 : 25), $\chi^2 = 0.55$, $P > 0.05$), suggesting that the male-sterile phenotype was controlled by a single, recessive gene.

To characterize cytological defects, transverse sections of WT and *Osalkbh5* anthers at different developmental stages (Zhang *et al.*, 2011) were prepared and analyzed. No morphological differences were observed from Stages 7 to 9, covering generation of pollen mother cells and four somatic cell layers, meiosis to produce microsporocytes in tetrads, microspore release from the tetrad, and initial condensation and degeneration of tapetal layers

Fig. 1 Phenotypic and transverse section analysis of *Osalkbh5* mutants. (a–c) Wild-type (WT), *Osalkbh5-1*, and *Osalkbh5-2* mutant plants at flowering stage (a), flowers after removal of palea and lemma (b), and anthers (c). Bars: (a) 10 cm; (b) 500 μm; (c) 200 μm. (d) I_2–KI staining of WT, *Osalkbh5-1*, and *Osalkbh5-2* pollen. Dark staining indicates viable pollen. Bar, 100 μm. (e–p) Transverse sections of WT (e–h), *Osalkbh5-1* (i–l), and *Osalkbh5-2* (m–p) anthers from Stages 10 to 13. Bars, 25 μm. Dbs, debris; DM, degraded microspore; E, epidermis; En, endothecium; Mp, mature pollen; Msp, microspore; T, tapetum.

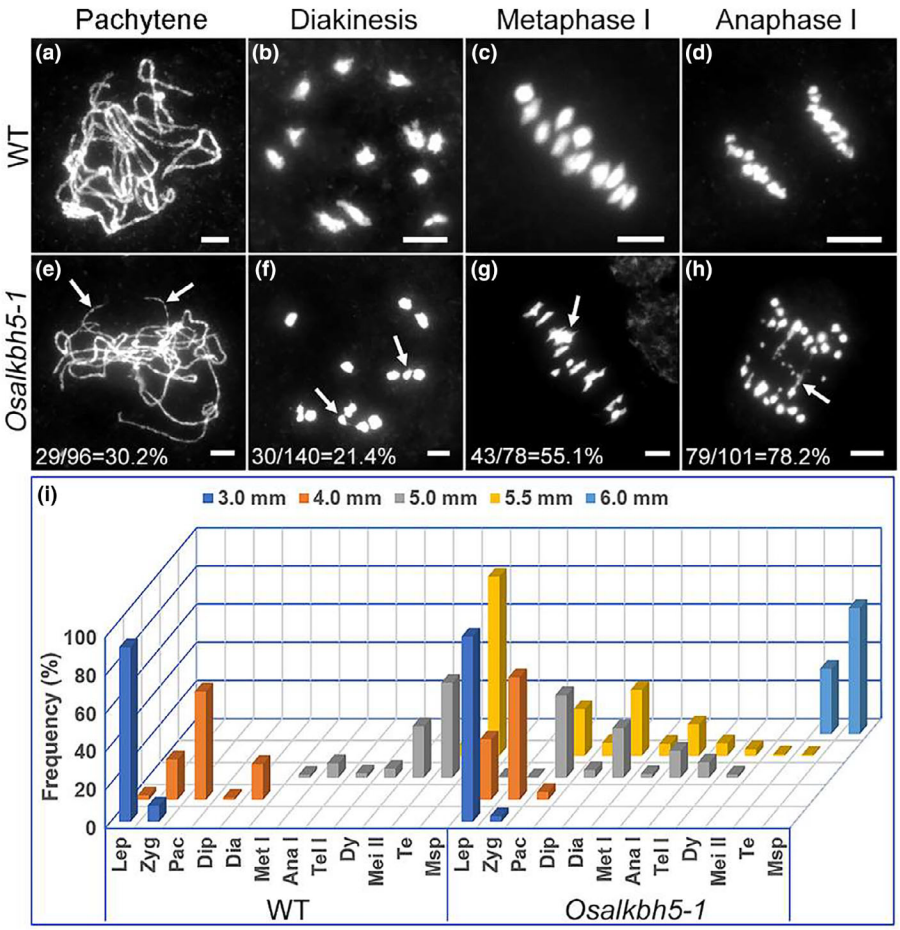

Fig. 2 Progression of meiosis is impeded in *Osalkbh5* mutants. (a–h) Meiotic wild-type (WT) (a–d) and *Osalkbh5-1* (e–h) chromosomes. Arrows indicate unsynapsed chromosomes at pachytene (e); abnormal chromosome associations and univalents at diakinesis (f); an entangled mass at Metaphase I (g); and bridges and DNA fragmentations at Anaphase I (h). Percentages show defective/total meiocytes (e–h). Bars, 5 μm. (i) Distribution of meiotic phases of WT and *Osalkbh5-1* pollen mother cells (PMCs) at various lengths of flowers. Ana I, Anaphase I; Dia, diakinesis; Dip, diplotene; Dy, dyads; Lep, leptotene; Mei II, meiosis II including Metaphase II, Anaphase II, Telophase II; Met I, Metaphase I; Msp, microspores; Pac, pachytene; Te, tetrads; Tel I, Telophase I; Zyg, zygotene. Bars of different colours represent PMCs at distinct developmental stages, juged by the length of flowers.

(Fig. S1). From Stage 10, WT tapetal cells condense, microspores enlarge and become vacuolated (Fig. 1e), undergo mitosis, and accumulate starch so that by maturity (Stage 13), WT anthers contain starchy pollen grains and tapetal cells that have almost entirely degenerated (Fig. 1f–h). By contrast, in *Osalkbh5* anthers, microspores apparently vacuolate successfully at Stage 10, but tapetal layers remain thick (Fig. 1i,m). In later stages, tapetal cells become abnormally vacuolated and swollen, and cytosolic constituents seem to bulge into the anther locule, while microspores exhibit irregular shapes and gradually collapse and degrade into deeply stained debris (Fig. 1j–l,n–p).

Meiotic chromosome behaviors are defective in *Osalkbh5* meiocytes

To ascertain whether male meiosis progresses normally in *Osalkbh5* meiocytes, chromosome behavior in WT and *Osalkbh5* pollen mother cells (PMCs) was investigated using DAPI staining. In WT cells, following chromatin condensation, homologous pairing, and synapsis, thick chromosomal threads were observed at late pachytene (Fig. 2a). The fully synapsed homologous chromosomes further condensed into 12 clear rod/ring-shaped bivalents at diakinesis (Fig. 2b) that aligned neatly along the equatorial plate (Fig. 2c), separating to opposite poles in Anaphase I and forming a dyad with equal numbers of chromosomes (Figs 2d, S2a). During the second meiotic division, sister chromatids of each chromosome segregated equally to give rise to tetrads (Fig. S2b) that are released as microspores with chromatids condensed into a central nucleus (Fig. S2c).

In *Osalkbh5* meiocytes, meiotic chromosomes displayed WT behavior until late pachytene, when unsynapsed chromosome regions remained as single, thin threads in *c.* 30% cells (n = 96; Fig. 2e). At diakinesis, univalents were observed in *c.* 20% of *Osalkbh5* PMCs (n = 140); meanwhile, nonhomologous associations were frequently observed (Fig. 2f). By Metaphase I, these irregular associations developed into clearly distinguishable entangled masses as a result of the pulling force of the spindle in 55.1% of *Osalkbh5* PMCs (n = 78; Fig. 2g). Chromosome fragmentation and bridges appeared in most *Osalkbh5* PMCs (*c.* 80%, n = 101) during chromosome segregation (Fig. 2h), leading to unequal distribution of chromosome numbers and randomly distributed lagging chromosomes in dyads and tetrads, thereby resulting in abnormal microspores with micronuclei and aneuploid numbers of chromosomes (Fig. S2d–f).

We further examined the progression of meiosis during WT and *Osalkbh5* anther development. Meiosis initiated normally in 3.0 mm flowers in both lines, but while most WT meiocytes progressed to pachytene in 4.0 mm flowers, *Osalkbh5* meiocytes mainly stayed in zygotene. In 5.0 mm flowers, WT meiocytes rapidly progressed beyond meiosis and produced tetrads. By contrast, most *Osalkbh5* meiocytes remained at earlier meiotic stages

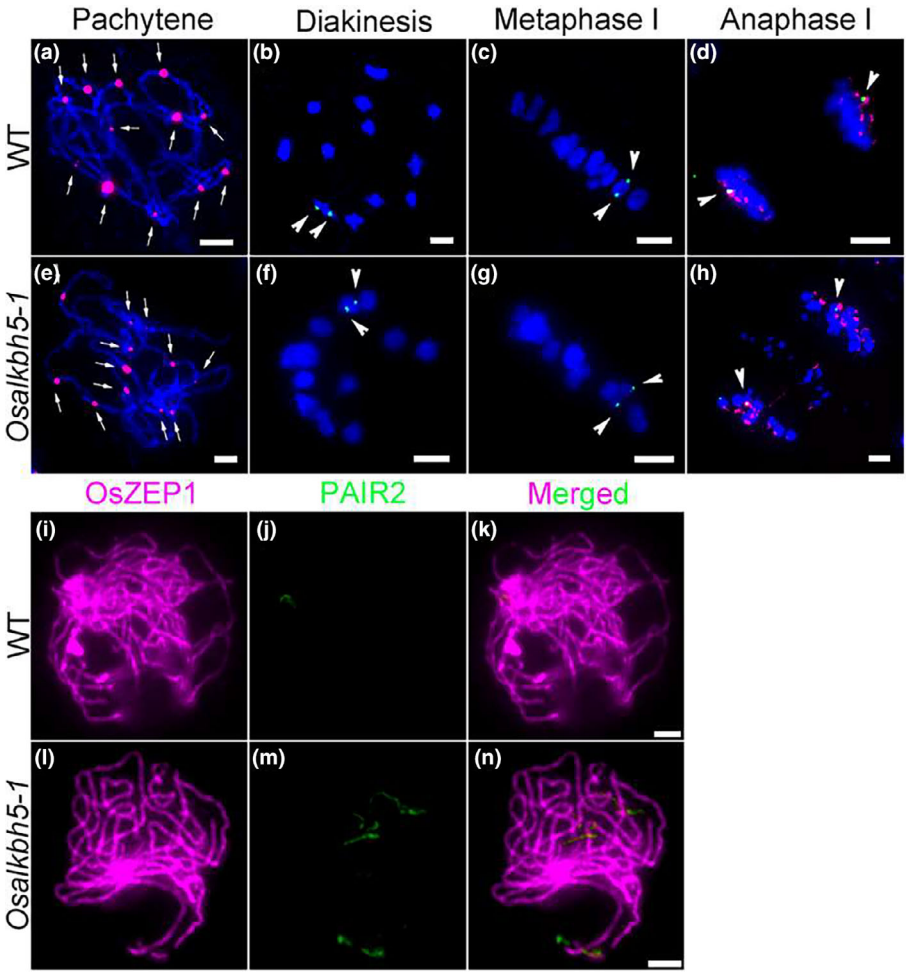

Fig. 3 *Osalkbh5* meiocytes display defective synapses with normal homologous pairing. (a–h) Chromosomes analyzed by fluorescence *in situ* hybridization (FISH) using Cy3-labeled CentO (magenta) and fluorescein isothiocyanate (FITC)-labeled 5S rDNA (green) probes. Arrows indicate CentO sites in (a, e), and 5S rDNA sites in (b–d, f–h). Bars, 5 μm. (i–n) Dual-immunolocalization analysis of OsZEP1 (magenta) and PAIR2 (green) in wild-type (WT) and *Osalkbh5-1* meiocyte nuclei at late pachytene. Bars, 2 μm.

until flower length reached 6.0 mm (Fig. 2i). These results indicate that *OsALKBH5* is required for accurate and timely meiotic progression.

Synapsis is partially compromised in *Osalkbh5* meiocytes

The visible chromosomal defects observed in *Osalkbh5* meiocytes hinted at aberrant DSB repair and CO formation. In most organisms, errors in chromosome pairing and synapsis generally impair homologous recombination. We monitored homologous pairing using FISH, using a fluorescein isothiocyanate (FITC)-labeled 5S rDNA (repetitive DNA) probe to a region near the centromere on the short arm of chromosome 11; and a Cy3-labeled CentO probe that targets the centromeric regions of all rice chromosomes. During pachytene, 12 CentO signals were detected in both WT and *Osalkbh5* meiocytes, suggesting successful homologous pairing (Fig. 3a,e). Subsequently, the paired 5s rDNA region within a distinguishable bivalent migrated to the opposite poles of the cell in both lines (Fig. 3b–d,f–h), but a lagging chromosome without a CentO signal appeared trapped near the equatorial plate (Fig. 3h), suggesting that acentric chromosome fragments are produced in *Osalkbh5* meiocytes.

Homologous synapsis ends with the assembly of the synaptonemal complex (SC) along the whole length of the homologs. The SC enhances the close attachment of homologous chromosomes in Prophase I and consists of a central element (CE) and two parallel axial/lateral elements (AEs/LEs). To investigate whether SC assembly was efficient in *Osalkbh5* meiocytes, dual-immunolocalization using antibodies against OsZEP1 (CE protein), PAIR2 (associated with unsynapsed AEs), and PAIR3 (associated with both unsynapsed AEs and LEs) together with REC8 (indicative of early Prophase I chromosomes) were performed in both *Osalkbh5* and WT PMCs (Nonomura *et al.*, 2006; Wang *et al.*, 2010, 2011). In WT cells, OsZEP1 was detected as short linear signals at zygotene, and fully colocalized with REC8 linear signals along the entire chromosome at pachytene (Fig. S3a,b). PAIR2 signals were spread along the chromosomes, and diminished from zygotene to pachytene (Fig. S3e,f), while PAIR3 signals gradually increased to be evenly distributed along the entire chromosome at pachytene (Fig. S3i,j). Similar patterns and progression of the distributions of these three SC proteins were observed in *Osalkbh5* cells at these meiotic stages (Fig. S3c,d,g,h,k,l). However, in late pachytene, WT PAIR2 signals gradually disappeared (Fig. 3i–k), but in *Osalkbh5*, *c.* 24% PMCs (n = 37) displayed obvious PAIR2 stretches not aligned with OsZEP1 signals (Fig. 3l–n). Mutation of OsALKBH5 therefore does not appear to inhibit homologous pairing and bivalent formation, but impairs full-length synapsis.

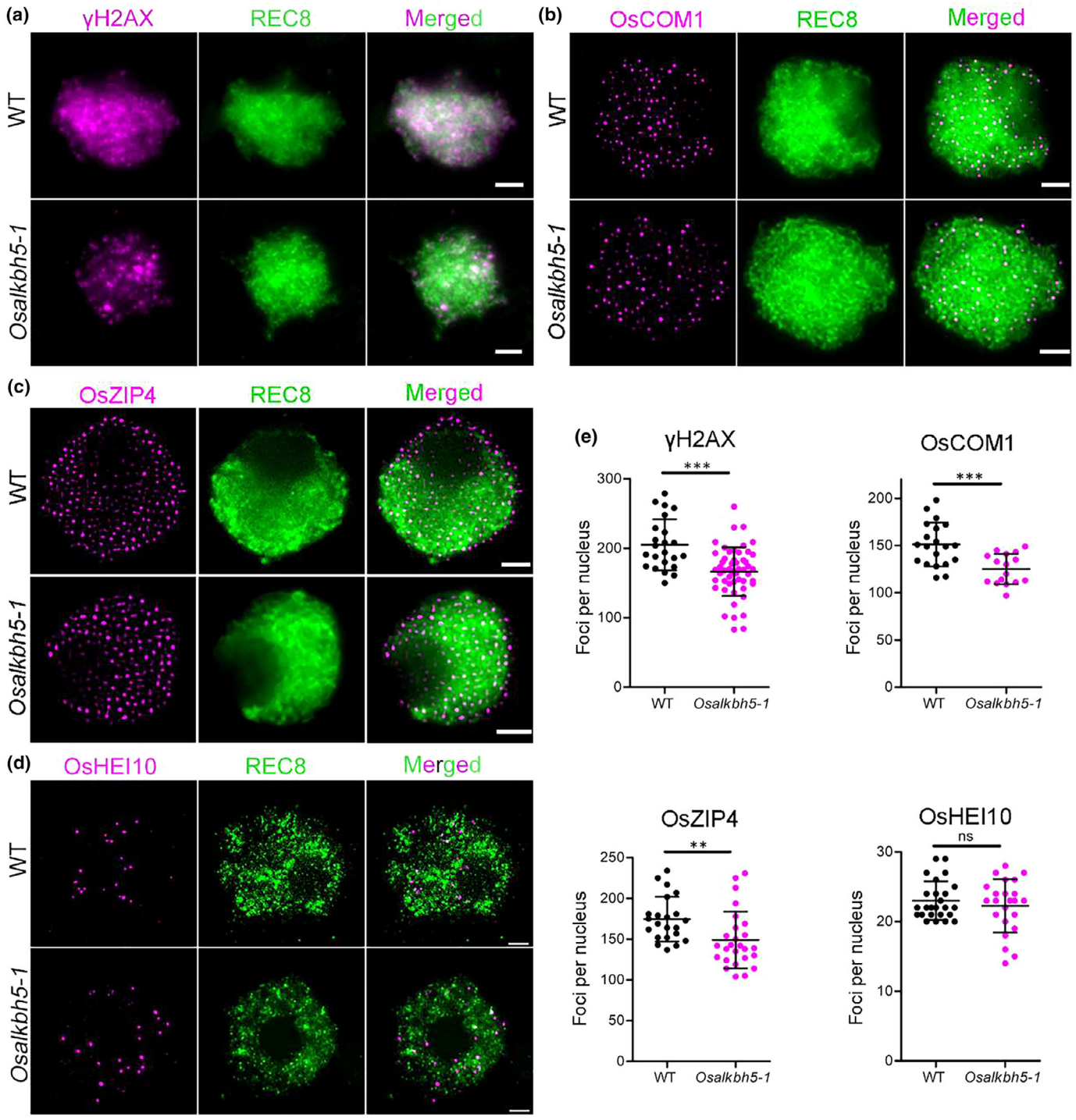

Fig. 4 Dual-immunolocalization analysis of *Osalkbh5-1*. (a–d) Immunofluorescence of γH2AX (a; leptotene), OsCOM1 (b; zygotene), OsZIP4 (c; zygotene), and OsHEI10 (d; diakinesis) signals in wild-type and *Osalkbh5-1* meiocytes. (e) Statistical analysis of numbers of γH2AX (a), OsCOM1 (b), OsZIP4 (c), OsHEI10 (d) signals in wild-type and mutant meiotic cells. REC8 signals indicate meiotic chromosomes. All values are represented by mean ± SD. Asterisks indicate significant differences (two-tailed Student's *t*-test; **, $P < 0.01$; ***, $P < 0.0001$); ns, no significant difference. Bars, 5 μm.

DSB formation and repair is disturbed in *Osalkbh5* meiocytes

To investigate the effect of OsALKBH5 disruption on DSB formation, we employed a dual-immunolocalization assay using antibodies against REC8 and γH2AX (phosphorylated H2AX), which marks DSB sites (Hunter *et al.*, 2001). A decreased number of γH2AX foci were observed in *Osalknh5* meiocytes during early Prophase I (166 ± 1.9 in *Osalknh5* vs 208 ± 1.9 in WT; Fig. 4a,e), indicating a

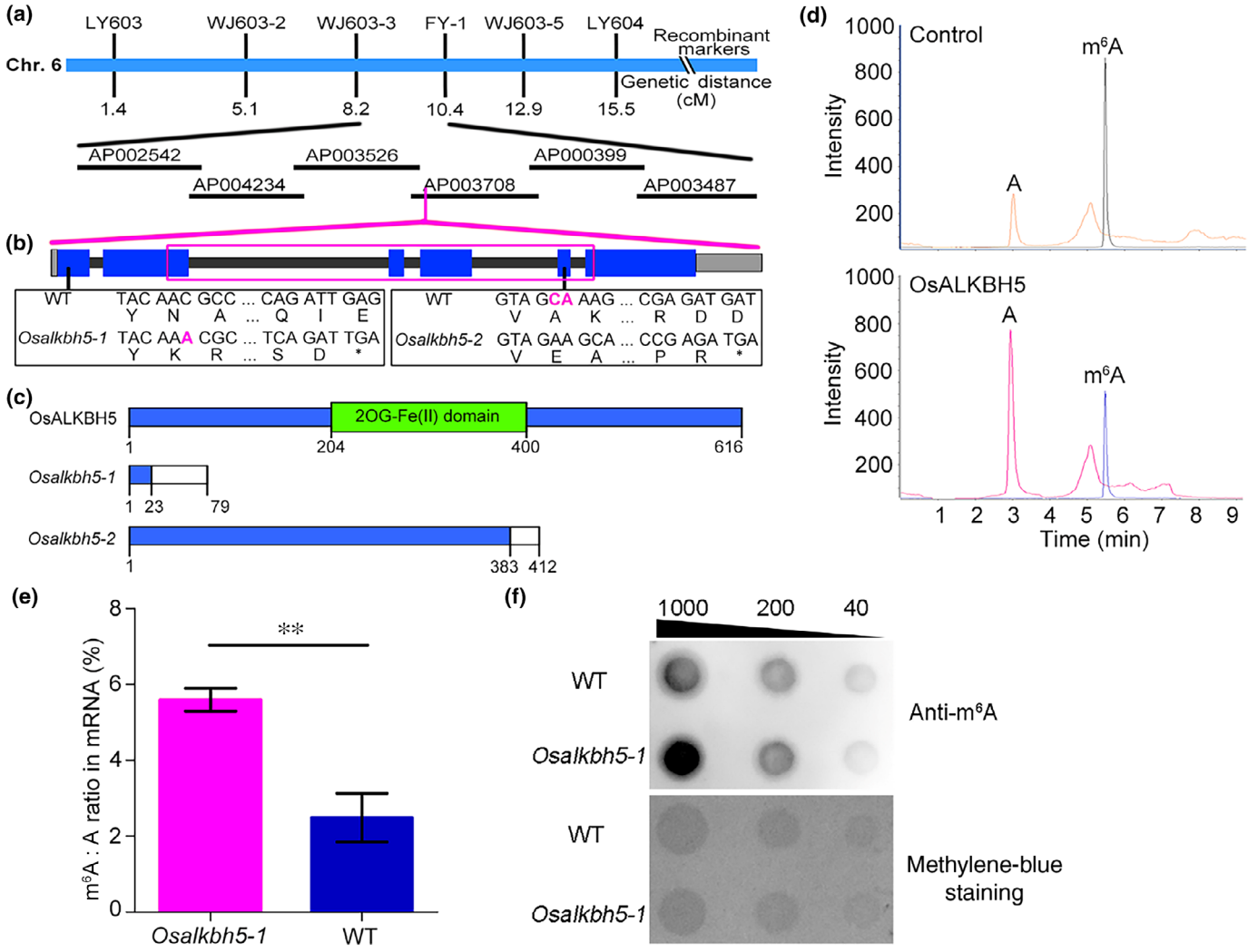

Fig. 5 Map-based cloning and characteristics of *OsALKBH5*. (a) Fine mapping of *Osalkbh5* mutants, showing names and positions of molecular markers. AP002542–AP003487, rice genomic DNA accession numbers of bacterial artificial chromosomes. Magenta line in AP003378 indicates the site of mutative gene. cM, centimorgans. (b) Gene structure of *OsALKBH5*. Blue and gray boxes represent exons and untranslated regions, respectively, while the black lines represent introns. The magenta box indicates the conserved genomic DNA domain. Black boxes show insertion and deletion sites (in magenta) of *Osalkbh5* mutants. (c) Schematic representation of predicted wild-type (WT) and mutant OsALKBH5 proteins. Blue boxes represent WT sequences, with the green box indicating the conserved 2OG-Fe (II) oxygenase domain. White boxes depict mutant protein sequences. Numbers represent the positions of amino acids within OsALKBH5 protein. (d) LC-MS/MS chromatograms of digested substrates after incubation of the m^{6}A-containing ssRNA with OsALKBH5. (e) Quantification of the N^6-methyladenosine (m^{6}A) : A ratio in messenger RNA (mRNA) of WT and *Osalkbh5* anthers using LC-MS/MS. Error bars are mean ± SD of two technical replicates and three biological replicates. Asterisks indicate significant differences (two-tailed Student's *t*-test; **, $P < 0.01$). (f) Dot-blot analysis of m^{6}A levels in mRNAs of *Osalkbh5-1* and WT anthers. The top panel is the dot-blot detection using anti-m^{6}A antibody, while the panel below is the methylene-blue staining result of the same membrane after blot. Numbers at the top represent the amount of mRNA (ng).

significantly lower level of meiotic DSB formation in *Osalkbh5* lines.

In rice, DSB resection by OsCOM1 (SAE2 homolog) generates the 3′-single-stranded DNA for target template invasion to repair broken DNA (Ji *et al.*, 2012). The average number of OsCOM1 foci in *Osalknh5* meiocytes was also significantly lower in zygotene (125.1 ± 4.0 in *Osalkbh5* cells vs 151.1 ± 5.2 in WT; Fig. 4b,e). OsZIP4, as a ZMM protein, has been reported to control obligatory CO formation in rice (Shen *et al.*, 2012; Wang *et al.*, 2012); its presence was also reduced in *Osalknh5* meiocytes at zygotene (149.0 ± 6.8 in *Osalkbh5* cells vs 176.4 ± 5.8 in WT; Fig. 4c,e). OsHEI10, another ZMM protein, elongates along the chromosomes, condenses at chiasmata during late Prophase I, and is used to label the class I CO (> 90% of total CO) in rice (Wang *et al.*, 2012). At diakinesis, while the mean numbers of OsHEI10 foci were similar in WT and *Osalkbh5* meiocytes, the number of OsHEI10 foci in *Osalkbh5* cells showed a much larger variation (14–28 per *Osalkbh5* cell vs 20–29 per WT cell; Fig. 4d,e). These results suggest that OsALKBH5 regulates the homologous recombination pathway for faithful DSB repair.

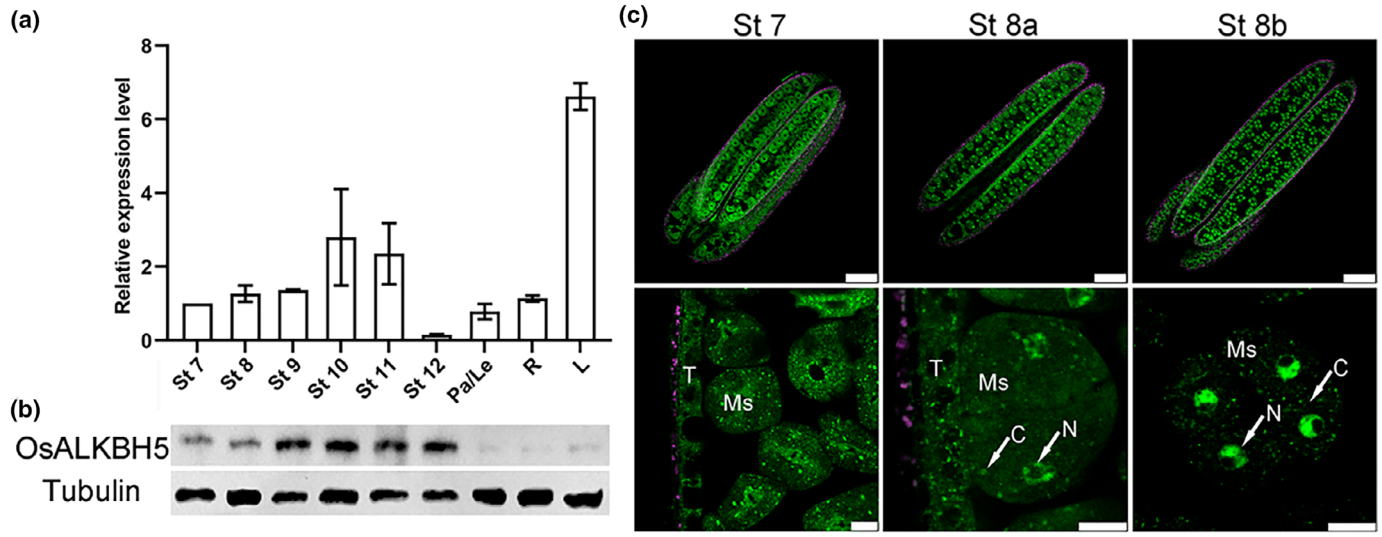

Fig. 6 *OsALKBH5* is widely expressed, while its protein is enriched in anthers. (a) Spatial and temporal expression analysis of *OsALKBH5* by RT-qPCR. Data show mean ± SD of three biological replicates, relative to *OsActin* expression. L, seedling leaf; Pa/Le, palea and lemma; R, seedling root; St 7–12, stages of anther development. (b) OsALKBH5 protein expression in the same tissues, detected with anti-OsALKBH5 antibody. (c) Fluorescence signals of eGFP-tagged *OsALKBH5*, with expression driven by its native promoter in a null *Osalkbh5* background. C, cytoplasm; Ms, microsporocyte; N, nucleus; St, stage; T, tapetal cell. Bars: (upper) 100 μm; (lower) 10 μm.

Map-based cloning of *OsALKBH5*

To identify the mutant gene of *Osalkbh5*, a map-based cloning approach was adopted, and the mutation site of *Osalkbh5-1* or *Osalkbh5-2* was mapped between two markers, WJ603-3 and FY-1 of chromosome 6 (Fig. 5a). High-throughput sequencing revealed a single A insertion after the 68th nucleotide in Exon 1 of *Os06g0138200* (LOC_*Os06g04660*) in *Osalkbh5-1*, and a two base-pair deletion ($C^{1148}A^{1149}$) in the fifth exon of the same gene in *Osalkbh5-2* (Fig. 5b). Both mutations caused frame shifts and premature translational termination, as well as complete disappearance of the protein (Figs 5c, S4). To further confirm that these mutations cause the observed phenotype, a 7266-bp WT genomic fragment of *Os06g0138200* was introduced into *Osalkbh5-1* mutant plants. I_2-KI staining showed that the fertility of transgenic plants was restored (Fig. S5), demonstrating that *Os06g0138200* is the causative gene underlying the male-sterile *Osalkbh5* phenotype.

OsALKBH5 is an m^{6}A-mRNA demethylase

The protein encoded by *Os06g0138200* is predicted to contain a 2OG-Fe (II) dependent oxygenase domain. Phylogenetic analysis indicates that OsALKBH5 clusters with ALKBH5 homologs from humans (Hs), *Arabidopsis* (At), and tomato (Sl) (Fig. S6), suggesting that OsALKBH5 may possess m^{6}A demethylation activity. In rice, four genes encode ALKBH5-like proteins: OsALKBH5 clustered with the ALKBH9 subclade in *Arabidopsis* and shared highest sequence similarity with AtALKBH9B, whereas the other three homologs clustered with the ALKBH10 subclade (Figs S6, S7).

To test whether OsALKBH5 acts as an RNA demethylase, tagged rice and human proteins were purified from *E. coli* and tested in catalytic reactions against a standard m^{6}A-containing single-stranded RNA substrate (Jia *et al.*, 2011; Zheng *et al.*, 2013). Compared with the negative control (no ALKBH5), m^{6}A abundance decreased after 2-h incubation with OsALKBH5, in line with reductions observed with the HsALKBH5 positive control (Figs 5d, S8). Furthermore, both quantitative analysis and dot-blot analysis showed significantly increased m^{6}A levels in mRNA of *Osalkbh5-1* compared with WT anthers (Fig. 5e,f). Taken together, these results demonstrate that OsALKBH5 functions as an m^{6}A-RNA demethylase in rice.

OsALKBH5 is enriched in anthers and localized in the nucleus and cytoplasm

Reverse transcription quantitative PCR analysis revealed that *OsALKBH5* is broadly expressed in anthers and other tissues such as leaves, roots, and palea/lemma (Fig. 6a). In anthers, *OsALKBH5* mRNA generally increased until Stage 10 and then decreased, while protein levels tended to stay high after Stage 10 (Fig. 6b). However, despite mRNA expression in vegetative tissues – very high in seedling leaves – OsALKBH5 protein was poorly expressed outside anthers (Fig. 6a,b).

To confirm these results, an enhanced GFP (eGFP)-tagged genomic *OsALKBH5* sequence was introduced into *Osalkbh5-1* calli; transgenic plants with restored male fertility showed clear fluorescent signals in anthers (Fig. 6c). Interestingly, the fluorescent signals existed as speckles located in the cytoplasm and nucleoplasm of PMCs, microspores, and tapetal cells. Subcellular localization analysis using rice protoplasts or tobacco (*N. benthamiana* L.) leaves confirmed the location of OsALKBH5 in both the cytoplasm and nucleoplasm (Fig. S9). This finding contrasts with the human and *Arabidopsis* homologs, as HsALKBH5 occurs in the nucleus, while AtALKBH9B is

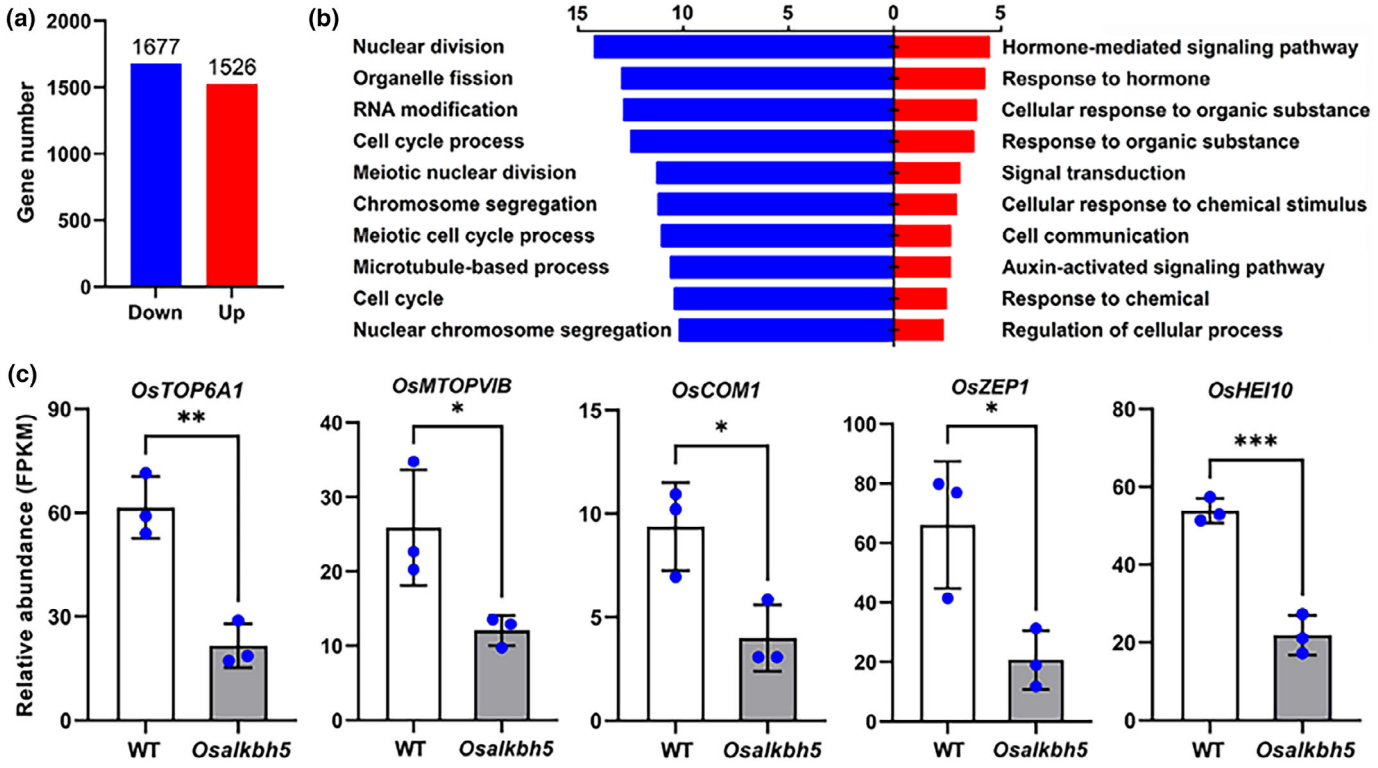

Fig. 7 Transcriptome profiles are dramatically changed in early Prophase I *Osalkbh5* meiocytes. (a) Differentially expressed genes (DEGs) in wild-type (WT) vs *Osalkbh5* meiocytes. (b) Gene Ontology (GO) analysis of DEGs, showing the top 10 GO terms in genes upregulted (red bars) and downregulated (blue bars) in the *Osalkbh5* mutant relative to the WT. The numbers calculated by $-10 \times \log_{10}(P\text{-value})$ represent enrichment of the terms. (c) Relative expression of representative downregulated genes. Data indicate mean ± SD of FPKM from three biological replicates of sequencing. Asterisks indicate significant differences (two-tailed Student's *t*-test; *, $P < 0.05$; **, $P < 0.01$; ***, $P < 0.0001$). FPKM, fragments per kilobase per million mapped reads.

found in cytoplasmic bodies (Zheng *et al.*, 2013; Martínez-Pérez *et al.*, 2017).

OsALKBH5 is colocalized with RNA processing bodies

To determine the precise intracellular location of OsALKBH5, a OsALKBH5-YFP fusion protein was transiently co-expressed with mCherry-tagged OsMAGO1, a core subunit of the exon junction complex (EJC); or OsDCP1-1, an ortholog of AtDCP1, a decapping enzyme located in cytoplasmic P-bodies that contain mRNA (Xu *et al.*, 2006; Gong & He, 2014). The fluorescent signals showed that OsALKBH5 granules colocalized precisely with OsDCP1-1 in the cytoplasm, and partially associated with OsMAGO1 in both the nucleus and cytoplasm (Fig. S10). These results suggested that OsALKBH5 may contribute to the EJC and P-bodies, participating in the metabolism of target mRNAs.

OsALKBH5 is involved in mRNA stability regulation

To explore how OsALKBH5 influences mRNA processing, highly pure WT and *Osalkbh5* meiocytes at early Prophase I were collected and sequenced to identify DEGs. In total, 3203 DEGs were identified, with 1526 upregulated and 1677 downregulated genes in the mutant line (Fig. 7a). Gene Ontology enrichment analysis showed that upregulated DEGs were mainly associated with hormone-mediated signaling or responses to organic/chemical stimuli; while downregulated DEGs were mainly involved in nuclear division, RNA processing, or meiotic processes and chromosome segregation (Fig. 7b). These data demonstrate dramatically changed transcriptome profiles in *Osalkbh5* relative to WT PMCs.

A closer look at specific genes revealed that dozens of genes crucial to early meiotic events were downregulated, such as *OsTOP6A1*, *OsMTOPVIB*, *OsCOM1*, *OsZEP1*, and *OsHEI10* (Table 1; Fig. 7c). The functions of their encoded proteins in DSB formation, resection and synapsis are consistent with the phenotypes observed in *Osalkbh5* mutants, strongly indicating that OsALKBH5 plays vital roles in early meiosis by regulating mRNA stability.

OsALKBH5 regulates post-transcriptional processing by m^{6}A-RNA demethylation

To investigate how OsALKBH5 affects meiotic progression, m^{6}A-RNA immunoprecipitation sequencing (MeRIP-seq) analysis was performed during meiosis from WT and *Osalkbh5*, and the peaks were filtered using the criteria of fold change (FC) ≥ 2

Table 1 Differentially expressed and/or methylated genes critical to meiotic Prophase I.

Gene	Locus	RNA-seq (log_2FC)	MeRIP-seq (m^6A FC)
DSB formation			
OsTOP6A1	Os03g0752200	−1.56	0.52
OsBVF1	Os05g0251400	−1.82	0.48
OsMTOPVIB	Os06g0708200	−1.00	0.59
DSB-ends resection and strand invasion			
OsBRCA2	Os01g0164800	−1.13	0.61
OsCOM1	Os06g0613400	−1.51	4.42
RPA2C	Os06g0693300	−1.06	0.59
Pairing and synapsis			
ZYGO1	Os01g0219200	−2.51	0.51
OsZEP1	Os04g0452500	−1.66	2.03
PAIR2	Os09g0506800	−0.82	2.21
PAIR3	Os10g0405500	−1.52	1.73
Homologous recombination safeguard genes			
OsTOP3α	Os03g0165000	−2.19	0.74
OsRecQl4	Os04g0433800	−1.02	0.64
OsMHF2	Os04g0481500	−1.46	0.42
OsMSH2	Os05g0274200	−1.00	3.55
CO formation			
HEIP1	Os01g0167700	−1.98	1.79
OsZIP4	Os01g0890900	−1.10	2.95
OsHEI10	Os02g0232100	−1.29	0.68
OsMER3	Os02g0617500	−2.29	0.54
OsSHOC1	Os02g0642600	−1.17	0.66

CO, crossover; DSB, double-stranded break; FC, fold change. Changes are for levels observed in the mutant relative to the wild-type (WT).

and score $(-10 \times \log_{10}(P\text{-value})) \geq 50$. The observed peaks were spread across the full length of the gene, mainly in the 3′-untranslated region (UTR) and coding sequence (CDS), with enrichment around stop and start codons, as well as a minority in the 5′UTR (Fig. 8a). Two strongly conserved motifs – UGKAS and DGGACU (K = G or A, S = G or C, D = U, A or G) – were identified around methylated A ribonucleotides (Fig. 8b).

To analyze the modification changes after mutation of *OsALKBH5*, DMGs were screened with FC ≥ 1.5, and identified 2576 transcripts with additional methylation, and 2230 transcripts with lower methylation levels in the mutant (Fig. 8c). Given that OsALKBH5 is a demethylase, m^6A levels of target RNAs should be increased after mutation. Therefore transcripts with additional methylation – those that are likely the targets of OsALKBH5 activity – were subject to GO analysis, which revealed that these genes were predominantly involved in processes including protein transport, DNA and RNA metabolism, translation, and DSB repair (Fig. 8d).

To investigate whether the altered m^6A methylation affects gene expression, joint analysis of the differential methylated genes from the MeRIP-seq and transcriptome profiles was performed. There were 230 and 381 genes overlapped between DEGs and up- or down-DMGs, suggesting that differential methylation may have indirect effects on mRNA abundance (Fig. S11a,b). Nonetheless, dozens of these overlapped genes, especially the downregulated DEGs, were enriched in cell cycle and meiotic events (Fig. S11c,d; Table 1).

Finally, we assessed whether OsALKBH5 may interact directly with transcripts of *PAIR2*, *PAIR3*, *OsCOM1*, *OsZIP4*, and *HEIP1* by RIP-qPCR from *OsALKBH5-eGFP* complemented plants. All of these genes were downregulated DEGs and up-methylated DMGs (Table 1); and all were shown to be direct targets of OsALKBH5 (Fig. 9a,b). These results indicate that OsALKBH5 may contribute directly to mRNA stability by mediating m^6A modification, to directly and indirectly influence phenotypes (Fig. 10). Other genes

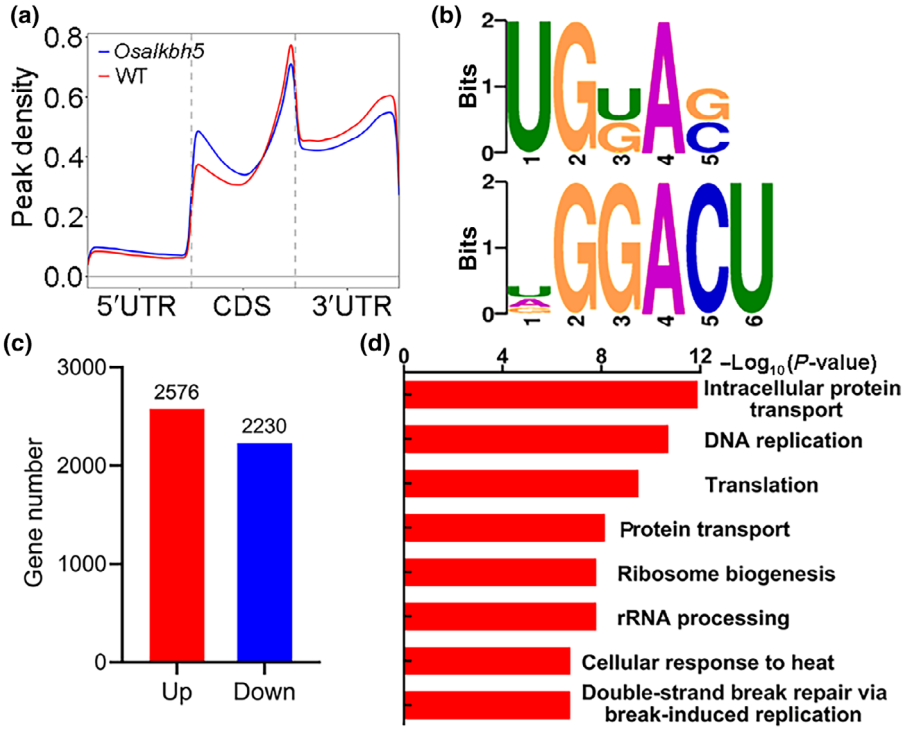

Fig. 8 MeRIP-seq analysis shows altered N^6-methyladenosine (m^6A) profiles in *Osalkbh5* meiocytes. (a) Metagene profiles of the distribution (density) of m^6A peaks across a gene. CDS, coding sequence; UTR, untranslated region. (b) Sequence logo representing consensus motifs of m^6A modification of all identified peaks. (c) Differentially methylated gene (DMG) numbers in *Osalkbh5* compared with wild-type (WT) with fold change ≥ 1.5 and $P \leq 0.001$ (n = 3 biological replicates). (d) Top 10 significantly enriched Gene Ontology (GO) terms for DMGs with additional methylation in *Osalkbh5* lines.

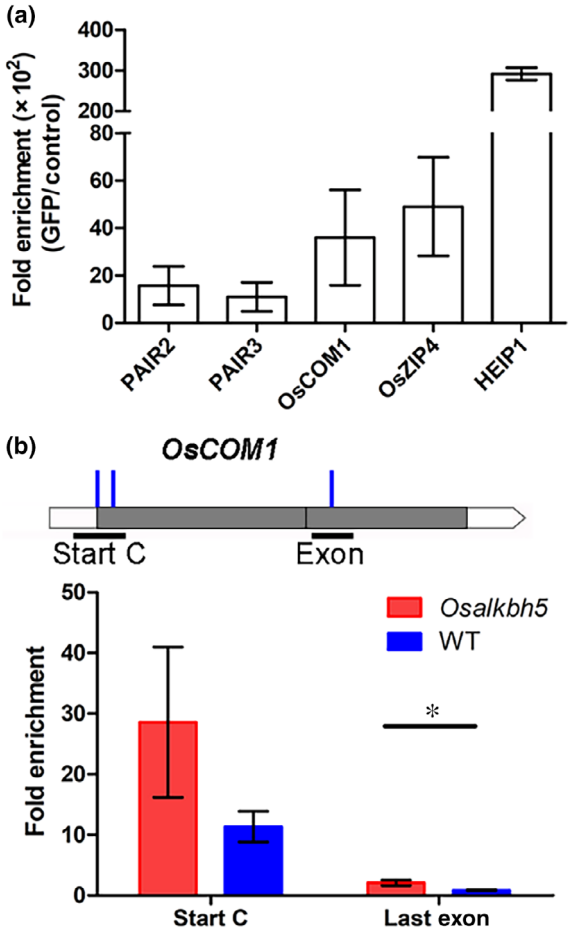

Fig. 9 OsALKBH5 directly binds transcripts of core meiotic genes. (a) *In vivo* binding of OsALKBH5 to transcripts in *OsALKBH5-eGFP* plants (RIP-qPCR). The *y*-axis shows the relative enrichment of selected genes in transgenic plants (normalized to input). Data are represented as mean ± SD, $n = 3$ technical replicates × 2 biological replicates. (b) N^6-methyladenosine (m^6A) peaks enrichment in *OsCOM1* transcripts (MeRIP-seq). Blue lines represent m^6A positions and fold enrichment is presented as mean ± SD of three biological replicates. The asterisk indicates significant difference (two-tailed Student's *t*-test; *, $P < 0.05$). Start C, translation start coden; WT, wild-type.

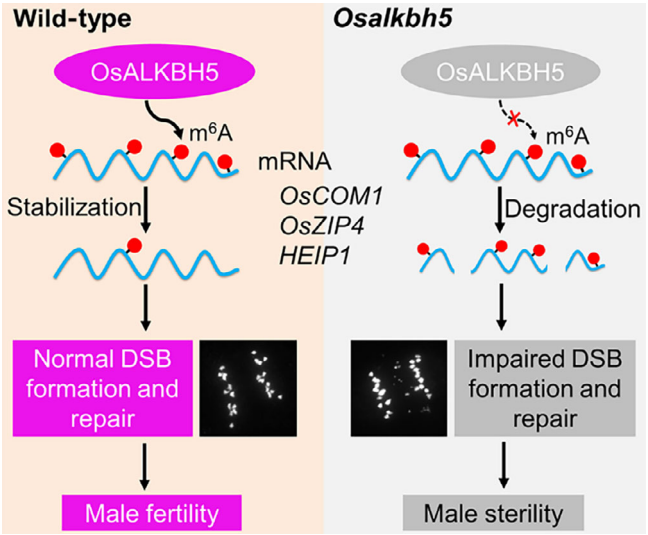

Fig. 10 Proposed working model of OsALKBH5 in rice meiotic progression. In wild-type male meiotic cells (left panel), OsALKBH5 removes the N^6-methyladenosine (m^6A) modification on several meiotic genes, including *OsCOM1*, *OsZIP4*, *HEIP1*, and possibly other genes involved in double-strand break (DSB) formation and repair. This stabilizes the messenger RNA (mRNA) of these genes and promotes meiotic progression, especially the DSB formation and repair process. Failure of m^6A erasure in *Osalkbh5* mutants (right panel) causes retention of more m^6A and decay of targeted transcripts, leading to defective meiotic progression and male sterility. Red dots represent m^6A modification sites on mRNA. Red X mark with dotted arrow indicates disturbed process.

involved in early meiotic events, such as *OsMTOPVIB*, *OsBRCA2*, *OsHEI10*, and *OsMER3*, which showed reduced mRNA abundance and decreased m^6A modification (Table 1), present intriguing candidates for further study, to reveal how knockout of a demethylase can reduce methylation of certain mRNA transcripts.

Discussion

m^6A is the most abundant RNA modification in eukaryotes, including plants, and is dynamically deposited and removed (Shi *et al.*, 2019; Shao *et al.*, 2021). ALKBH5 and its homologs have been demonstrated to play conserved roles in m^6A demethylation (an 'eraser') in both animals and plants. Although the functions of m^6A erasers are well documented in dicot plants (Duan *et al.*, 2017; Martínez-Pérez *et al.*, 2017; Amara *et al.*, 2022), their roles in monocot plants, including cereal crops, is relatively understudied. Here, we demonstrate that m^6A demethylation mediated by OsALKBH5 is essential for meiotic progression and male fertility in rice.

OsALKBH5 is essential for meiotic DSB formation and repair

Osalkbh5 mutants showed defective meiotic-specific phenotypes, suggesting that normal progression of rice meiosis is OsALKBH5-dependent. The most obvious cytological defects during Prophase I of *Osalkbh5* lines were production of a mixture of multivalents and univalents at diakinesis, as well as DNA fragmentation after male meiotic chromosome segregation (Fig. 2f–h). *OsALKBH5* mutations did not block homologous pairing and had only mild effects on SC formation (Figs 3, S3). Immunolocalization results indicated a decreased amount of DSBs evidenced by reduced γH2AX foci (Fig. 4a). Furthermore, insufficient chromosomal loading of DSB repair protein OsCOM1 was also detected in the *Osalkbh5* mutant (Fig. 4b). These results suggest that OsALKBH5 is mainly involved in regulating DSB formation and repair.

Previous results showed that mutations in OsFIP37, a key component of the 'writer' complex in rice, lead to arrest of meiosis at a much earlier stage (F. Zhang *et al.*, 2019). In *Osfip37* meiocytes, homologous chromosomes do not undergo pairing but become aggregated at diakinesis, followed by fragmentation and degradation at Metaphase I. By contrast, *Osalkbh5* mutants

were able to produce tetrads and microspores (Figs S1, S2). In addition, OsFIP37 and its partner OsFAP1 (OsFIP37-associated protein 1) have been demonstrated to regulate male meiosis by promoting local auxin levels in the anther (Cheng *et al.*, 2022), while our study proposes that OsALKBH5 directly regulates the mRNA stability of meiotic genes. Similarly, in mammals, the m^{6}A methyltransferase METTL3 and demethylase ALKBH5 operate in mitotic spermatogonia and meiotic spermatogenic cells, respectively. Inactivation of METTL3 in mice causes a much earlier meiotic arrest compared with *alkbh5* knockout mice (Zheng *et al.*, 2013; Xu *et al.*, 2017). Collectively, the difference in the phenotypic defects may reflect the stage-specific roles of m^{6}A deposition and removal during meiosis.

Except for the meiotic defects, tapetal cells exhibit delayed degeneration and irregular morphology in *Osalkbh5* mutants after Stage 10 (Fig. 1i–p). Besides, *OsALKBH5* is also preferentially expressed in the tapetum during the meiotic and postmeiotic stages (Fig. 6c). Furthermore, *OsALKBH5* is kept highly expressed in the anther until Stage 11 (Fig. 6a). These results indicate that OsALKBH5 may also play a role in programmed cell death (PCD) of the tapetal layer.

OsALKBH5 is required for m^{6}A-mediated post-transcriptional regulation of meiotic genes

Phylogenetic and *in vitro* assays established that OsALKBH5 is a m^{6}A demethylase (Figs 5d–f, S6). A comparison of changes in expression and m^{6}A levels of transcripts in mutant male meiocytes indicates that disruption of OsALKBH5 affects m^{6}A abundance, perturbing mRNA decay of several key genes related to meiotic Prophase I (Figs 7, 8; Table 1), leading to delayed and defective meiotic progression (Figs 2, S2).

It has been shown that many meiotic genes are expressed before meiosis initiation and that some show differential transcript abundance at different meiotic stages (Fujita *et al.*, 2010; Barakate *et al.*, 2021). These observations strongly suggest that post-transcriptional regulation plays essential roles in controlling the activity of meiotic genes, of which m^{6}A modification is an important element. In mice, both the 'writer' METTL3 and 'eraser' ALKBH5 have been reported to regulate mRNA splicing and stability. Our results showed that multiple meiosis-specific genes related to DSB formation and repair show increased m^{6}A levels and reduced RNA abundance in the *Osalkbh5* mutant (Table 1). However, a large number of meiosis-specific genes, while also downregulated in expression in the *Osalkbh5* mutant, showed decreased m^{6}A methylation (Table 1), creating a rich field for further exploration.

Previous research has reported conflicting effects of m^{6}A levels on RNA abundance. Disruption of m^{6}A demethylase ALKBH10B resulted in increased m^{6}A and accelerated mRNA decay of the flowering activator FT and its upregulators *SPL3* and *SPL9*, thereby delaying flowering in *Arabidopsis* (Duan *et al.*, 2017). Mutants of m^{6}A methyltransferase FIO1 in *Arabidopsis* showed a decrease in global m^{6}A mRNA methylation and increase in expression of a central flowering integrator *SUPPRESSOR OF OVEREXPRESSION OF CONSTANS 1* (*SOC1*) and its direct repressor *SHORT VEGETATIVE PHASE* (*SVP*), resulting in an early-flowering phenotype (Xu *et al.*, 2022). Similarly, knocking out m^{6}A methyltransferase subunit *OsFIP* resulted in decreased methylation levels and upregulated targeted NTPase genes (F. Zhang *et al.*, 2019), but dissociation of OsFIP37 caused by loss of function of OsFAP1 abolished m^{6}A deposition on *OsYUCCA3* mRNAs that downregulated *OsYUCCA3* expression (Cheng *et al.*, 2022). Taken together with our results, these findings show that the effects of m^{6}A on downstream molecular pathways are heterogeneous, in line with the opinion that the mechanisms depend on context (Z. Zhang *et al.*, 2020). Regardless of the mechanism, we have shown that OsALKBH5 is a new factor required for meiotic progress, and likely works by regulating transcript stability of target meiosis-specific genes via m^{6}A modification to direct faithful completion of meiosis and ensure male fertility.

Acknowledgements

We thank Zhijin Luo, Mingjiao Chen, and Zibo Chen (Shanghai Jiao Tong University) for mutant screening and generation of F2 populations for mapping. We thank Prof. Hongquan Yang and Dr Pengbo Xu (Shanghai Jiao Tong University) for the supply of PHB-YFP/mCherry vectors. We would like to thank Dr Wei Zhang for LC-MS/MS analysis in the Core Facility and Service Center (CFSC) for the School of Life Sciences and Biotechnology, SJTU. This work was supported by funds from the National Natural Science Foundation of China (U19A2031 and 32070608) and the Innovative Research Team, the Ministry of Education, and 111 Project (Grant B14016).

Competing interests

None declared.

Author contributions

WL, HG and IS designed the project. FX, JZ, DW, SS, MF and JW performed the experiments. FX, IS and WL wrote the paper. FX, JZ and DW contributed equally to this work.

ORCID

Ming Fu https://orcid.org/0009-0008-3762-5668
Hongbo Gao https://orcid.org/0000-0003-2013-5298
Wanqi Liang https://orcid.org/0000-0002-9938-5793
Iain Searle https://orcid.org/0000-0003-4306-9756
Shiyu Sun https://orcid.org/0000-0003-2836-9435
Jie Wang https://orcid.org/0009-0007-1970-8075
Di Wu https://orcid.org/0009-0000-8503-2164
Feiyang Xue https://orcid.org/0000-0002-8427-1195
Jie Zhang https://orcid.org/0000-0003-4725-8407

Data availability

The data that support the findings of this study are openly available in RAP-DB at http://rapdb.dna.affrc.go.jp and the PHYTOZOME at

https://phytozome-next.jgi.doe.gov under the following accession nos.: OsALKBH5 (Os06g0138200/LOC_Os06g04660), OsMago1 (Os08g0107900/LOC_Os08g01660), OsDCP1-1 (Os11g0155000/LOC_Os11g05650). Accession numbers for the other sequences used in the phylogenic analysis are listed on the tree. Sequence data of RNA-seq and MeRIP-seq from this article can be found in the GenBank data libraries under accession no.: PRJNA1125654 (https://www.ncbi.nlm.nih.gov/bioproject/PRJNA1125654).

References

Amara U, Shoaib Y, Kang H. 2022. ALKBH9C, a potential RNA m^{6}A demethylase, regulates the response of Arabidopsis to abiotic stresses and abscisic acid. *Plant, Cell & Environment* **45**: 3566–3581.

Arribas-Hernández L, Bressendorff S, Hansen MH, Poulsen C, Erdmann S, Brodersen P. 2018. An m^{6}A-YTH module controls developmental timing and morphogenesis in Arabidopsis. *Plant Cell* **30**: 952–967.

Barakate A, Orr J, Schreiber M, Colas I, Lewandowska D, McCallum N, Macaulay M, Morris J, Arrieta M, Hedley PE *et al.* 2021. Barley anther and meiocyte transcriptome dynamics in meiotic prophase I. *Frontiers in Plant Science* **11**: 619404.

Bart R, Chern M, Park CJ, Bartley L, Ronald PC. 2006. A novel system for gene silencing using siRNAs in rice leaf and stem-derived protoplasts. *Plant Methods* **2**: 13.

Bergerat A, de Massy B, Gadelle D, Varoutas P-C, Nicolas A, Forterre P. 1997. An atypical topoisomerase II from archaea with implications for meiotic recombination. *Nature* **386**: 414–417.

Bishop DK, Zickler D. 2004. Early decision: meiotic crossover interference prior to stable strand exchange and synapsis. *Cell* **1**: 9–15.

Cannavo E, Reginato G, Cejka P. 2019. Stepwise 5' DNA end-specific resection of DNA breaks by the Mre11-Rad50-Xrs2 and Sae2 nuclease ensemble. *Proceedings of the National Academy of Sciences, USA* **116**: 5505–5513.

Chang G, Shi L, Ye Y, Shi H, Zeng L, Tiwary S, Huse JT, Huo L, Ma L, Ma Y *et al.* 2020. YTHDF3 induces the translation of m^{6}A-enriched gene transcripts to promote breast cancer brain metastasis. *Cancer Cell* **38**: 857–871.

Chelysheva L, Vezon D, Chambon A, Gendrot G, Pereira L, Lemhemdi A, Vrielynck N, Le Guin S, Novatchkova M, Grelon M. 2012. The Arabidopsis HEI10 is a new ZMM protein related to Zip3. *PLoS Genetics* **8**: e1002799.

Chen L, Chu H, Yuan Z, Pan AH, Liang W, Huang H, Shen MS, Zhang DB. 2006. Isolation and genetic analysis for rice mutants treated with ^{60}Co-γ ray. *Journal of Xiamen University* **45**: 82–85.

Cheng P, Bao S, Li C, Tong J, Shen L, Yu H. 2022. RNA N^6-methyladenosine modification promotes auxin biosynthesis required for male meiosis in rice. *Developmental Cell* **57**: 1–14.

Du H, Zhao Y, He J, Zhang Y, Xi H, Liu M, Ma J, Wu L. 2016. YTHDF2 destabilizes m^{6}A-containing RNA through direct recruitment of the CCR4-NOT deadenylase complex. *Nature Communications* **7**: 12626–12636.

Duan H-C, Wei L-H, Zhang C, Wang Y, Chen L, Lu Z, Chen PR, He C, Jia G. 2017. ALKBH10B is an RNA N^6-methyladenosine demethylase affecting Arabidopsis floral transition. *Plant Cell* **29**: 2995–3011.

Fu M, Wang C, Xue F, Higgins J, Chen M, Zhang D, Liang W. 2016. The DNA topoisomerase VI-B subunit OsMTOPVIB is essential for meiotic recombination initiation in rice. *Molecular Plant* **9**: 1539–1541.

Fu R, Wang C, Shen H, Zhang J, Higgins JD, Liang W. 2020. Rice OsBRCA2 is required for DNA double-strand break repair in meiotic cells. *Frontiers in Plant Science* **11**: 600820.

Fu Y, Luo GZ, Chen K, Deng X, Yu M, Han D, Hao Z, Liu J, Lu X, Dore LC *et al.* 2015. N^6-methyldeoxyadenosine marks active transcription start sites in *Chlamydomonas*. *Cell* **161**: 879–892.

Fujita M, Horiuchi Y, Ueda Y, Mizuta Y, Kubo T, Yano K, Yamaki S, Tsuda K, Nagata T, Niihama M *et al.* 2010. Rice expression atlas in reproductive development. *Plant and Cell Physiology* **51**: 2060–2081.

Gong P, He C. 2014. Uncovering divergence of rice exon junction complex core heterodimer gene duplication reveals their essential role in growth, development, and reproduction. *Plant Physiology* **165**: 1047–1061.

Greer EL, Blanco MA, Gu L, Sendinc E, Liu J, Aristizabal-Corrales D, Hsu CH, Aravind L, He C, Shi Y. 2015. DNA methylation on N^6-adenine in *C. elegans*. *Cell* **161**: 868–878.

He Y, Wang C, Higgins JD, Yu J, Zong J, Lu P, Zhang D, Liang W. 2016. MEIOTIC F-BOX is essential for male meiotic DNA double-strand break repair in rice. *Plant Cell* **28**: 1879–1893.

Hinch AG, Becker PW, Li T, Moralli D, Zhang G, Bycroft C, Green C, Keeney S, Shi Q, Davies B *et al.* 2020. The configuration of RPA, RAD51, and DMC1 binding in meiosis reveals the nature of critical recombination intermediates. *Molecular Cell* **79**: 689–701.

Hsu PJ, Zhu Y, Ma H, Guo Y, Shi X, Liu Y, Qi M, Lu Z, Shi H, Wang J *et al.* 2017. Ythdc2 is an N^6-methyladenosine binding protein that regulates mammalian spermatogenesis. *Cell Research* **27**: 1115–1127.

Hunter N, Börner GV, Lichten M, Kleckner N. 2001. Gamma-H2AX illuminates meiosis. *Nature Genetics* **27**: 236–238.

Ji J, Tang D, Wang K, Wang M, Che L, Li M, Cheng Z. 2012. The role of OsCOM1 in homologous chromosome synapsis and recombination in rice meiosis. *The Plant Journal* **72**: 18–30.

Jia G, Fu Y, Zhao X, Dai Q, Zheng G, Yang Y, Yi C, Lindahl T, Pan T, Yang YG *et al.* 2011. N^6-methyladenosine in nuclear RNA is a major substrate of the obesity-associated FTO. *Nature Chemical Biology* **7**: 885–887.

Jiang P, Lian B, Liu C, Fu Z, Shen Y, Cheng Z, Qi Y. 2020. 21-nt phasiRNAs direct target mRNA cleavage in rice male germ cells. *Nature Communications* **11**: 5191.

Li H, Kim YJ, Yang L, Liu Z, Zhang J, Shi H, Huang G, Persson S, Zhang D, Liang W. 2020. Grass-specific EPAD1 is essential for pollen exine patterning in rice. *Plant Cell* **32**: 3961–3977.

Li N, Zhang DS, Liu HS, Yin CS, Li XX, Liang WQ, Yuan Z, Xu B, Chu HW, Wang J *et al.* 2006. The rice tapetum degeneration retardation gene is required for tapetum degradation and anther development. *Plant Cell* **18**: 2999–3014.

Li Y, Qin B, Shen Y, Zhang F, Liu C, You H, Du G, Tang D, Cheng Z. 2018. HEIP1 regulates crossover formation during meiosis in rice. *Proceedings of the National Academy of Sciences, USA* **115**: 10810–10815.

Li Y, Wang X, Li C, Hu S, Yu J, Song S. 2014. Transcriptome-wide N^6-methyladenosine profiling of rice callus and leaf reveals the presence of tissue-specific competitors involved in selective mRNA modification. *RNA Biology* **11**: 1180–1188.

Liu B, Merriman DK, Choi SH, Schumacher MA, Plangger R, Kreutz C, Horner SM, Meyer KD, Al-Hashimi HM. 2018. A potentially abundant junctional RNA motif stabilized by m^{6}A and Mg^{2+}. *Nature Communications* **9**: 2761.

Liu C, Shen Y, Qin B, Wen H, Cheng J, Mao F, Shi W, Tang D, Du G, Li Y *et al.* 2020. *Oryza sativa* RNA-dependent RNA polymerase 6 contributes to double-strand break formation in meiosis. *Plant Cell* **32**: 3273–3289.

Liu J, Yue Y, Han D, Wang X, Fu Y, Zhang L, Jia G, Yu M, Lu Z, Deng X *et al.* 2014. A METTL3-METTL14 complex mediates mammalian nuclear RNA N^6-adenosine methylation. *Nature Chemical Biology* **10**: 93–95.

Liu L, Zhang Y, Tang S, Zhao Q, Zhang Z, Zhang H, Dong L, Guo H, Xie Q. 2010. An efficient system to detect protein ubiquitination by agroinfiltration in *Nicotiana benthamiana*. *The Plant Journal* **61**: 893–903.

Liu N, Dai Q, Zheng G, He C, Parisien M, Pan T. 2015. N^6-methyladenosine-dependent RNA structural switches regulate RNA-protein interactions. *Nature* **518**: 560–564.

Martínez-Pérez M, Aparicio F, López-Gresa MP, Bellés JM, Sánchez-Navarro JA, Pallás V. 2017. Arabidopsis m^{6}A demethylase activity modulates viral infection of a plant virus and the m^{6}A abundance in its genomic RNAs. *Proceedings of the National Academy of Sciences, USA* **114**: 10755–10760.

Meyer KD, Patil DP, Zhou J, Zinoviev A, Skabkin MA, Elemento O, Pestova TV, Qian S-B, Jaffrey SR. 2015. 5′ UTR m^{6}A promotes cap-independent translation. *Cell* **163**: 999–1010.

Meyer KD, Saletore Y, Zumbo P, Elemento O, Mason CE, Jaffrey SR. 2012. Comprehensive analysis of mRNA methylation reveals enrichment in 3′ UTRs and near stop codons. *Cell* **149**: 1635–1646.

Nonomura K-I, Nakano M, Eiguchi M, Suzuki T, Kurata N. 2006. PAIR2 is essential for homologous chromosome synapsis in rice meiosis I. *Journal of Cell Science* **119**: 217–225.

Ping XL, Sun BF, Wang L, Xiao W, Yang X, Wang WJ, Adhikari S, Shi Y, Lv Y, Chen YS *et al.* 2014. Mammalian WTAP is a regulatory subunit of the RNA N^6-methyladenosine methyltransferase. *Cell Research* **24**: 177–189.

Růžička K, Zhang M, Campilho A, Bodi Z, Kashif M, Saleh M, Eeckhout D, El-Showk S, Li H, Zhong S *et al.* 2017. Identification of factors required for m^6A mRNA methylation in Arabidopsis reveals a role for the conserved E3 ubiquitin ligase HAKAI. *New Phytologist* **215**: 157–172.

Scutenaire J, Deragon JM, Jean V, Benhamed M, Raynaud C, Favory JJ, Merret R, Bousquet-Antonelli C. 2018. The YTH domain protein ECT2 is an m^6A reader required for normal trichome branching in Arabidopsis. *Plant Cell* **30**: 986–1005.

Shao Y, Wong CE, Shen L, Yu H. 2021. N^6-methyladenosine modification underlies messenger RNA metabolism and plant development. *Current Opinion in Plant Biology* **63**: 102047.

Shen H, Luo B, Wang Y, Li J, Hu Z, Xie Q, Wu T, Chen G. 2022. Genome-wide identification, classification and expression analysis of m^6A gene family in *Solanum lycopersicum*. *International Journal of Molecular Sciences* **23**: 4522.

Shen L, Liang Z, Gu X, Chen Y, Teo ZW, Hou X, Cai WM, Dedon PC, Liu L, Yu H. 2016. N^6-methyladenosine RNA modification regulates shoot stem cell fate in *Arabidopsis*. *Developmental Cell* **38**: 186–200.

Shen L, Liang Z, Yu H. 2017. Dot blot analysis of N^6-methyladenosine RNA modification levels. *Bio-Protocol* **7**: e2095.

Shen Y, Tang D, Wang K, Wang M, Huang J, Luo W, Luo Q, Hong L, Li M, Cheng Z. 2012. ZIP4 in homologous chromosome synapsis and crossover formation in rice meiosis. *Journal of Cell Science* **125**: 2581–2591.

Shi H, Wang X, Lu Z, Zhao BS, Ma H, Hsu PJ, Liu C, He C. 2017. YTHDF3 facilitates translation and decay of N^6-methyladenosine-modified RNA. *Cell Research* **27**: 315–328.

Shi H, Wei J, He C. 2019. Where, when, and how: context-dependent functions of RNA methylation writers, readers, and erasers. *Molecular Cell* **74**: 640–650.

Tang C, Klukovich R, Peng H, Wang Z, Yu T, Zhang Y, Zheng H, Klungland A, Yan W. 2018. ALKBH5-dependent m^6A demethylation controls splicing and stability of long 3'-UTR mRNAs in male germ cells. *Proceedings of the National Academy of Sciences, USA* **115**: E325–E333.

Vrielynck N, Chambon A, Vezon D, Pereira L, Chelysheva L, De Muyt A, Mézard C, Mayer C, Grelon M. 2016. A DNA topoisomerase VI–like complex initiates meiotic recombination. *Science* **351**: 939–943.

Wang C, Higgins JD, He Y, Lu P, Zhang D, Liang W. 2017. Resolvase OsGEN1 mediates DNA repair by homologous recombination. *Plant Physiology* **173**: 1316–1329.

Wang K, Wang M, Tang D, Shen Y, Miao C, Hu Q, Lu T, Cheng Z. 2012. The role of rice HEI10 in the formation of meiotic crossovers. *PLoS Genetics* **8**: e1002809.

Wang K, Wang M, Tang D, Shen Y, Qin B, Li M, Cheng Z. 2011. PAIR3, an axis-associated protein, is essential for the recruitment of recombination elements onto meiotic chromosomes in rice. *Molecular Biology of the Cell* **22**: 12–19.

Wang M, Wang K, Tang D, Wei C, Li M, Shen Y, Chi Z, Gu M, Cheng Z. 2010. The central element protein ZEP1 of the synaptonemal complex regulates the number of crossovers during meiosis in rice. *Plant Cell* **22**: 417–430.

Wang X, Lu Z, Gomez A, Hon GC, Yue Y, Han D, Fu Y, Parisien M, Dai Q, Jia G *et al.* 2014. N^6-methyladenosine-dependent regulation of messenger RNA stability. *Nature* **505**: 117–120.

Wang X, Zhao BS, Roundtree IA, Lu Z, Han D, Ma H, Weng X, Chen K, Shi H, He C. 2015. N^6-methyladenosine modulates messenger RNA translation efficiency. *Cell* **161**: 1388–1399.

Wei LH, Song P, Wang Y, Lu Z, Tang Q, Yu Q, Xiao Y, Zhang X, Duan HC, Jia G. 2018. The m^6A reader ECT2 controls trichome morphology by affecting mRNA stability in Arabidopsis. *Plant Cell* **30**: 968–985.

Wu Y, Xu X, Qi M, Chen C, Li M, Yan R, Kou X, Zhao Y, Liu W, Li Y *et al.* 2022. N^6-methyladenosine regulates maternal RNA maintenance in oocytes and timely RNA decay during mouse maternal-to-zygotic transition. *Nature Cell Biology* **24**: 917–927.

Xiao CL, Zhu S, He M, Chen Zhang Q, Chen Y, Yu G, Liu J, Xie SQ, Luo F, Liang Z *et al.* 2018. N^6-methyladenine DNA modification in the human genome. *Molecular Cell* **71**: 306–318.

Xiao W, Adhikari S, Dahal U, Chen YS, Hao YJ, Sun BF, Sun HY, Li A, Ping XL, Lai WY *et al.* 2016. Nuclear m^6A reader YTHDC1 regulates mRNA splicing. *Molecular Cell* **61**: 507–519.

Xing D, Wang Y, Hamilton M, Ben-Hur A, Reddy AS. 2015. Transcriptome-wide identification of RNA targets of Arabidopsis SERINE/ARGININE-RICH45 uncovers the unexpected roles of this RNA binding protein in RNA processing. *Plant Cell* **27**: 3294–3308.

Xu J, Yang JY, Niu QW, Chua NH. 2006. *Arabidopsis* DCP2, DCP1, and VARICOSE form a decapping complex required for postembryonic development. *Plant Cell* **18**: 3386–3398.

Xu K, Yang Y, Feng G-H, Sun B-F, Chen J-Q, Li Y-F, Chen Y-S, Zhang X-X, Wang C-X, Jiang L-Y *et al.* 2017. Mettl3-mediated m^6A regulates spermatogonial differentiation and meiosis initiation. *Cell Research* **27**: 1100–1114.

Xu T, Wu X, Wong CE, Fan S, Zhang Y, Zhang S, Liang Z, Yu H, Shen L. 2022. FIONA1-mediated m^6A modification regulates the floral transition in Arabidopsis. *Advanced Science* **9**: e2103628.

Yoo SD, Cho YH, Sheen J. 2007. Arabidopsis mesophyll protoplasts: a versatile cell system for transient gene expression analysis. *Nature Protocols* **2**: 1565–1572.

Zhang C, Chen L, Peng D, Jiang A, He Y, Zeng Y, Xie C, Zhou H, Luo X, Liu H *et al.* 2020. METTL3 and N^6-methyladenosine promote homologous recombination-mediated repair of DSBs by modulating DNA-RNA hybrid accumulation. *Molecular Cell* **79**: 425–442.

Zhang C, Chen Y, Sun B, Wang L, Yang Y, Ma D, Lv J, Heng J, Ding Y, Xue Y *et al.* 2017. m^6A modulates haematopoietic stem and progenitor cell specification. *Nature* **549**: 273–276.

Zhang D, Luo X, Zhu L. 2011. Cytological analysis and genetic control of rice anther development. *Journal of Genetics and Genomics* **38**: 379–390.

Zhang F, Zhang YC, Liao JY, Yu Y, Zhou YF, Feng YZ, Yang YW, Lei MQ, Bai M, Wu H *et al.* 2019. The subunit of RNA N^6-methyladenosine methyltransferase OsFIP regulates early degeneration of microspores in rice. *PLoS Genetics* **15**: e1008120.

Zhang G, Huang H, Liu D, Cheng Y, Liu X, Zhang W, Yin R, Zhang D, Zhang P, Liu J *et al.* 2015. N^6-methyladenine DNA modification in Drosophila. *Cell* **161**: 893–906.

Zhang J, Wang C, Higgins JD, Kim YJ, Moon S, Jung KH, Qu S, Liang W. 2019. A multiprotein complex regulates interference-sensitive crossover formation in rice. *Plant Physiology* **181**: 221–235.

Zhang S, Zhao BS, Zhou A, Lin K, Zheng S, Lu Z, Chen Y, Sulman EP, Xie K, Bogler O *et al.* 2017. m^6A demethylase ALKBH5 maintains tumorigenicity of glioblastoma stem-like cells by sustaining FOXM1 expression and cell proliferation program. *Cancer Cell* **31**: 591–606.

Zhang YC, Lei MQ, Zhou YF, Yang YW, Lian JP, Yu Y, Feng YZ, Zhou KR, He RR, He H *et al.* 2020. Reproductive phasiRNAs regulate reprogramming of gene expression and meiotic progression in rice. *Nature Communications* **11**: 6031–6041.

Zhang Z, Luo K, Zou Z, Qiu M, Tian J, Sieh L, Shi H, Zou Y, Wang G, Morrison J *et al.* 2020. Genetic analyses support the contribution of mRNA N^6-methyladenosine (m^6A) modification to human disease heritability. *Nature Genetics* **52**: 939–949.

Zhao BS, Wang X, Beadell AV, Lu Z, Shi H, Kuuspalu A, Ho RK, He C. 2017. m^6A-dependent maternal mRNA clearance facilitates zebrafish maternal-to-zygotic transition. *Nature* **542**: 475–478.

Zhao X, Yang Y, Sun BF, Shi Y, Yang X, Xiao W, Hao YJ, Ping XL, Chen YS, Wang WJ *et al.* 2014. FTO-dependent demethylation of N^6-methyladenosine regulates mRNA splicing and is required for adipogenesis. *Cell Research* **24**: 1403–1419.

Zheng G, Dahl JA, Niu Y, Fedorcsak P, Huang CM, Li CJ, Vagbo CB, Shi Y, Wang WL, Song SH *et al.* 2013. ALKBH5 is a mammalian RNA demethylase that impacts RNA metabolism and mouse fertility. *Molecular Cell* **49**: 18–29.

Zhong S, Li H, Bodi Z, Button J, Vespa L, Herzog M, Fray RG. 2008. MTA is an Arabidopsis messenger RNA adenosine methylase and interacts with a homolog of a sex-specific splicing factor. *Plant Cell* **20**: 1278–1288.

Zhou C, Wang C, Liu H, Zhou Q, Liu Q, Guo Y, Peng T, Song J, Zhang J, Chen L *et al.* 2018. Identification and analysis of adenine N^6-methylation sites in the rice genome. *Nature Plants* **4**: 554–563.

Zhou L, Tian S, Qin G. 2019. RNA methylomes reveal the m^6A-mediated regulation of DNA demethylase gene *SlDML2* in tomato fruit ripening. *Genome Biology* **20**: 156.

Supporting Information

Additional Supporting Information may be found online in the Supporting Information section at the end of the article.

Fig. S1 Transverse section analysis of wild-type (WT), *Osalkbh5-1*, and *Osalkbh5-2* anthers at Stages 7–9.

Fig. S2 Behavior of WT and *Osalkbh5-1* chromosomes in meiocytes and microspores.

Fig. S3 Dual-immunolocalization of OsZEP1, PAIR2, and PAIR3 in WT and *Osalkbh5-1* meiocytes.

Fig. S3 Dual-immunolocalization of OsZEP1, PAIR2, and PAIR3 in WT and *Osalkbh5-1* meiocytes. Bars, 5 μm.

Fig. S4 Detection of OsALKBH5 protein level in wild-type and *Osalkbh5* anthers.

Fig. S5 Phenotype comparison of WT and complemented plants (*OsALKBH5* gDNA introduced into *Osalkbh5-1* plants).

Fig. S6 Phylogenetic analysis of OsALKBH5 and homologs from *Arabidopsis thaliana* L. (At); *Oryza sativa* L. (Os); *Solanum lycopersicum* L. (Sl); *Homo sapiens* (Hs); and *Escherichia coli* (Es).

Fig. S7 Alignment of OsALKBH5 with 3 *Arabidopsis* homologs.

Fig. S8 LC-MS/MS chromatogram showing the retention times of adenosine (A) and N^6-methyladenosine (m^6A) nucleosides after incubation of the m^6A-containing ssRNA substrate with human ALKBH5 (HsALKBH5).

Fig. S9 Subcellular localization of OsALKBH5.

Fig. S10 Colocalization of OsALKBH5 (YFP) with OsMAGO1 and OsDCP1-1 (mCherry) in tobacco leaf.

Fig. S11 Joint analysis of MeRIP-seq and transcriptome profiles.

Table S1 Sequences of primers used in these experiments.

Please note: Wiley is not responsible for the content or functionality of any Supporting Information supplied by the authors. Any queries (other than missing material) should be directed to the *New Phytologist* Central Office.